UCSF
UC San Francisco Electronic Theses and Dissertations

Title
Targeting the Unfolded Protein Response in Pancreatic Neuroendocrine Tumors

Permalink
https://escholarship.org/uc/item/7v38v30g

Author
Qi, Jenny

Publication Date
2017

Peer reviewed|Thesis/dissertation

eScholarship.org Powered by the California Digital Library
University of California

Targeting the Unfolded Protein Response in Pancreatic Neuroendocrine Tumors

by

Jenny Qi

DISSERTATION

Submitted in partial satisfaction of the requirements for the degree of

DOCTOR OF PHILOSOPHY

in

Biomedical Sciences

in the

GRADUATE DIVISION

of the

UNIVERSITY OF CALIFORNIA, SAN FRANCISCO

Copyright 2017
by
Jenny Qi

Dedication and Acknowledgments

I dedicate this dissertation to the memory of my mother, Lisa Zhihong Yu.

Many thanks to my family and friends and the Parnassus Poets for their support over the years, with special thanks to David Watts, Wendy Chen, Evan Perkins, the graduate team of *Synapse*, and the folks at Bone Lab Radio.

I would like to acknowledge and thank Oakes and Papa Lab members past and present for discussion and support, especially my co-author Paul Moore for CRISP/Cas9 wizardry and sharing the burden of mouse injections, with special thanks also to Eric Wang, Anne Hiniker, Jason Nguyen, Elizabeth Earley, Adrienne Stormo, Maike Thamsen, and Rajarshi Ghosh; the Backes and Maley Labs for drug synthesis; Grace Kim and the UCSF Department of Pathology for human PanNET samples; Amy Chen and Lauren Rodda for friendship and brainstorming; the Krummel Lab (especially Ed Roberts) for good-humored discussion and mouse help; the Tlsty Lab (especially Joseph Caruso, Johnny Tse, and Chira Chen-Tanyolac) for NSG mice, immunohistochemistry protocols, and use of their microtome; the Berger Lab for RIP-Tag2 mice and protocols; Dr. Rushika Perera for technical assistance with RIP-Tag2 tumors; the Cyster Lab for use of their microscope; the Goga and Maltepe Labs for use of low-oxygen incubators; the Goga and Debnath Labs (especially Andrew Beardsley, Olga Momcilovic, Andrew Leidal, and Srirupa Roy) for antibodies, protocols, and discussion; the Weiss Lab (especially Wanlin Lo) for CRISPR plasmids; Vinh Nguyen for islet isolation; Peter Thompson of the Bhusan Lab for senescence stains; Lita and

Lorna Espinoza for lab maintenance; Dayi Su and Veronica Kuiper for NSG mouse care; the UCSF Diabetes Center and the UCSF Brain Tumor Research Center (BTRC) for tissue processing and sectioning, especially the Hebrok Lab, Debbie Ngow and King Chiu.

I would especially like to thank Matthias Hebrok, Andrei Goga, and my thesis advisor Scott Oakes, for serving on my thesis committee and providing constructive feedback and guidance. This project was truly a collaborative effort.

Targeting the Unfolded Protein Response in Pancreatic Neuroendocrine Tumors

Jenny Qi

Abstract

A critical regulator of the unfolded protein response (UPR), the IRE1α kinase/endoribonuclease promotes adaptation or apoptosis depending on the level of upstream endoplasmic reticulum (ER) stress. The UPR is implicated in multiple cancer types, but whether IRE1α signaling is beneficial or detrimental to tumor growth remains controversial. We hypothesized that pancreatic neuroendocrine tumors (PanNETs), which are highly secretory neoplasms prone to protein-folding stress, would be one type of cancer that would be particularly sensitive to changes in UPR signaling. We used a series of genetic and pharmacologic approaches to modulate IRE1α in xenograft and spontaneous genetic (RIP-Tag2) mouse models of PanNET. We found that IRE1α signaling is carefully titrated in PanNETs *in vivo* such that hyperactivating or inhibiting its enzymatic activity cripples tumor growth and survival. Importantly, we found that a monoselective IRE1α kinase inhibitor dramatically decreased tumor burden and prolonged animal survival in two preclinical PanNET models by eliminating the adaptive signals that would otherwise counteract an ER stress-induced apoptotic cascade. Here, I also present preliminary data suggesting that PanNETs may be similarly sensitive to modulation of PERK, a second regulatory arm of the UPR, as demonstrated by decreased tumor burden in response to both genetic and pharmacological inhibition of PERK. Our results provide a strong rationale for therapeutically targeting IRE1α in

PanNETs and other cancers that experience high levels of ER stress, as well as further investigations of the effects of targeting PERK.

Table of contents

Figures

Introduction

The Unfolded Protein Response determines cell fate in response to ER Stress

Over a third of all proteins in the mammalian cell, including nearly all secreted proteins, are co-translationally translocated into the endoplasmic reticulum (ER) as the first step in their journey through the secretory pathway. Once in the ER lumen, these proteins must be folded into their correct three-dimensional shapes and modified by chaperones, glycosylating enzymes, oxido-reductases, and other ER-localized enzymes (Sevier and Kaiser, 2002; Tu and Weissman, 2004). Despite these protein-folding efforts, it has been estimated that at least a third of all polypeptides are improperly folded, and for some proteins, the success rate is much lower (Schubert et al., 2000). Incompletely folded proteins are eliminated by quality control systems, including ER-associated degradation (ERAD) pathways (McCracken and Brodsky, 2003; Meusser et al., 2005; Smith et al., 2011).

When misfolded proteins in the ER accumulate above a critical threshold, a pathway called the unfolded protein response (UPR) is initiated to restore homeostasis. The UPR is initiated by three ER transmembrane proteins--inositol-requiring enzyme 1α (IRE1α; also known as ERN1), PRK-like ER kinase (PERK; also known as EIF2AK3), and activating transcription factor 6α (ATF6α)—that detect unfolded proteins and induce transcriptional and translational upregulation of components to expand ER protein folding capacity and decrease protein folding demand (Lerner et al., 2012; Meusser et al., 2005; Ron and Walter, 2007; Shore et al., 2011; Smith et al., 2011; Tabas and Ron,

2011). If ER stress levels are too severe or prolonged for these processes to restore homeostasis, the UPR regulators switch from a pro-homeostatic to pro-apoptotic state.

The most ancient ER stress sensor, **IRE1α**, is a critical life-death switch under conditions of ER stress. IRE1α contains an ER lumenal domain that directly binds unfolded proteins and dimerizes in response (Aragon et al., 2008, 2009; Credle et al., 2005; Zhou et al., 2006). On the cytosolic side, IRE1α has two distinct enzymatic domains—a serine/threonine kinase and endoribonuclease (RNase). Modulation of the auto-phosphorylation status of its kinase controls the activity and substrate specificity of the adjacent RNase domain to determine cell fate under ER stress (Han et al., 2009). Remediable ER stress (Figure 1A) causes low-level kinase auto-phosphorylation and dimerization this restricts IRE1α's RNase activity to a single adaptive substrate, *Xbp1* mRNA, from which it excises a 26-nt intron. Re-ligation of the 5- and 3- ends by RTCB shifts the mRNA into the open reading frame. Translation of spliced *Xbp1* produces the homeostatic transcription factor XBP1s

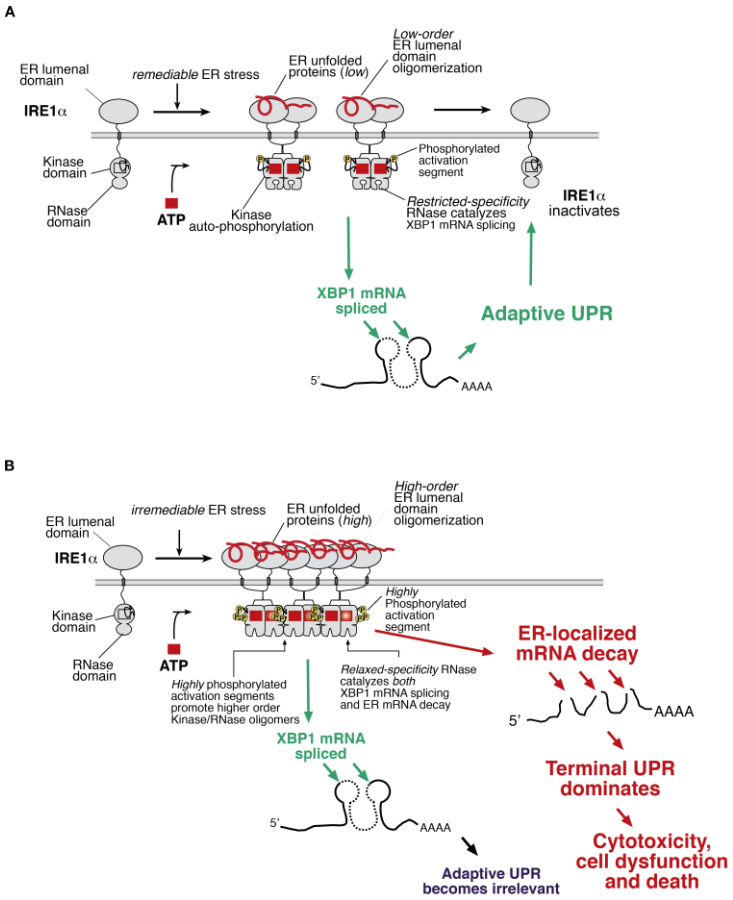

Figure 1: IRE1alpha determines cell fate in response to the level of ER stress in the cell

(s=spliced), which upregulates genes encoding ER protein-folding and quality control components, such as BiP/GRP78, culminating in the “Adaptive UPR” (Lee et al., 2003).

Under conditions of irremediable ER stress (Figure 1B), sustained, high-level kinase autophosphorylation causes higher order IRE1α oligomerization and relaxed specificity of IRE1α’s RNase, allowing it to endonucleolytically degrade many mRNAs at the ER membrane that encode secretory proteins, such as insulin (Han et al., 2009; Hollien et al., 2009), as well as essential components of the ER protein-folding machinery. The net consequence of high-level IRE1α RNase activation is that it promotes the deterioration of ER function. Moreover, hyperactivated IRE1α endonucleolytically degrades select microRNA precursors as a mechanism that upregulates key apoptotic signals, including Thioredoxin-Interacting Protein (TXNIP) (Lerner et al., 2012; Upton et al., 2012). Thus, hyperactive IRE1α RNase activity induces a “Terminal UPR,” whereby adaptive signaling through *Xbp1* splicing is eclipsed by pro-apoptotic signals (Upton et al., 2012).

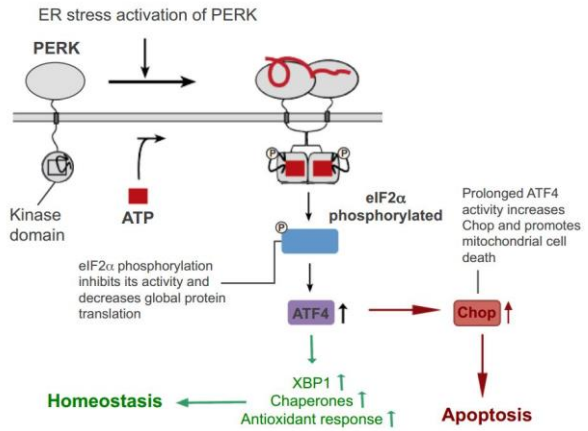

Figure 2. **PERK signaling determines cell fate**. (Left) Short-term activation of PERK decreases protein-folding demand and increases protein-folding capacity to promote homeostasis. (Right) Sustained PERK signaling triggers apoptosis.

PERK contains a cytosolic kinase whose signaling outputs contribute to both decreasing protein-folding demand and increasing protein-folding capacity in the ER. PERK phosphorylates eukaryotic translation initiation factor 2α (eIF2α), which inhibits assembly of the eIF2-GTP-Met-tRNA complex to slow down global protein

translation, including that of most Cap-dependent mRNAs (26, 27), thus decreasing protein-folding demand (28). At the same time, PERK actively promotes adaptation because eIF2α phosphorylation favors the internal ribosome entry site (IRES)-mediated translation of select mRNAs, such as that encoding activating transcription factor 4 (ATF4), a key adaptive output that transcriptionally upregulates genes involved in amino acid metabolism, oxidative stress resistance, and autophagy (29).

While a pause in overall protein translation can be beneficial for stressed cells by providing extra time to fold a backlog of proteins, a prolonged block in translation from sustained PERK signaling is inconsistent with survival. Therefore, ATF4 also increases the expression of the gene encoding CADD34, a major regulatory subunit of protein phosphatase 1 (PP1), which results in the dephosphorylation of eIF2α and restoration of mRNA translation (30). However, prolonged PERK activation also upregulates the transcription factor CHOP/GADD153, which inhibits expression of anti-apoptotic BCL-2 and increases expression of pro-apoptotic BCL2 family proteins to hasten cell death (31, 32). Hence, similar to IRE1α, PERK switches from Homeostatic to Terminal UPR under chronic ER stress.

The Unfolded Protein Response in Cancer

Tumor cells often invade foreign environments where unfavorable conditions, such as hypoxia, glucose deprivation, and inadequate amino acid supplies compromise protein-folding in the ER (Koumenis, 2006; Lee and Hendershot, 2006; Ma and Hendershot, 2004; Moenner et al., 2007). Moreover, cancer cells frequently harbor intrinsic stresses,

such as genomic instability and somatic mutations in client proteins of the secretory pathway that disrupt their folding and lead to ER stress (Dejeans et al., 2014; Horne et al., 2014; Ruggero, 2013; Tollefsbol and Cohen, 1990). It is therefore not surprising that many studies have shown evidence of sustained and high level UPR activity, including IRE1α activation, in various cancers, such as myeloma, glioblastoma, and carcinomas of the breast, stomach, esophagus, and liver (Carrasco et al., 2007; Chen et al., 2002; Fernandez et al., 2000; Gardner and Walter, 2011; Shuda et al., 2003; Song et al., 2001). In contrast, somatic mutations in the IRE1α pathway are rarely found (<1%) in these tumors, and most of these cases seem to be loss of function (Greenman et al., 2007; Xue et al., 2011). For example, we discovered that cancer-associated mutations in IRE1α selectively disable its apoptotic outputs while maintaining its homeostatic outputs (Ghosh et al., 2014), suggesting that some cancer cells evolve mechanisms to increase the ratio of the Adaptive/Terminal UPR to survive. Other studies have shown that IRE1α's homeostatic product XBP1s promotes tumor progression in models of triple-negative breast cancer (Chen et al., 2014), arguing that UPR signaling may be beneficial for tumor survival. However, whether the UPR ultimately inhibits or promotes solid tumor growth in patients remains an area of intense debate (Auf et al., 2010; Bobrovnikova-Marjon et al., 2010; Jamora et al., 1996; Oakes, 2017; Park et al., 2004; Romero-Ramirez et al., 2004).

Pancreatic Neuroendocrine Tumors

Given their high secretory activity, we predicted that pancreatic neuroendocrine tumors (PanNETs) would be one neoplasm that is particularly sensitive to protein-folding stress.

Not only do PanNETs universally hypersecrete one more peptide hormone(s) (Metz and Jensen, 2008; Oberg and Eriksson, 2005), but the endocrine cells of the pancreas from which these tumors derive are the cells in the body most impacted by genetic loss of the UPR in mice and humans (Delepine et al., 2000; Hassler et al., 2015; Lee et al., 2011). For the over 1,500 Americans diagnosed with a PanNET each year, surgery is the only potentially curative treatment. Unfortunately, the five year survival is extremely low for the ~25% of patients who develop metastatic disease(Metz and Jensen, 2008; Oberg and Eriksson, 2005). Hence, new targets are desperately needed for patients with advanced PanNETs.

We show here that ER stress-induced UPR activity is strongly unregulated in human PanNET samples and carefully titrated in a murine xenograft model to enhance the Adaptive UPR while preventing activation of the Terminal UPR. Using a variety of genetic and chemical tools, we discovered that disruption of this balance in UPR outputs is detrimental to tumor growth and survival. Forcibly engaging the Terminal UPR through hyperactivating IRE1α *in vivo* triggers apoptosis and decreases PanNET burden. Likewise, removing the Adaptive-UPR through genetic deletion of *Ire1α, Xbp1,* or *PERK* drastically reduces PanNET growth *in vivo*. Furthermore, administration of highly selective IRE1α and PERK kinase inhibitors phenocopies the antitumor effects of genetic deletion. The IRE1α inhibitor in particular demonstrates dramatic cytotoxic effects in two murine preclinical PanNET models without deleterious effects on animal health. Together, our data indicate that the UPR, especially its master regular IRE1α, is a promising therapeutic target in PanNETs and related ER stress-sensitive cancers.

Chapter 1: IRE1alpha signaling is skewed towards adaptation in cancers

Introduction

Homozygous genetic deletion of *Ire1α or Xbp1* during development or in adult β-cells results in β-cell dysfunction, defective insulin secretion and in the case of *Xbp1* deletion, β-cell death (Hassler et al., 2015; Lee et al., 2011; Tirasophon et al., 1998). These studies demonstrate that pancreatic neuroendocrine cells are critically dependent on the UPR for proper development and maintenance and gave us the idea of manipulating the UPR in pancreatic islet tumors.

While healthy endocrine cells secrete large amounts of protein in response to appropriate signals, the vast majority of both functioning and nonfunctioning PanNETs constitutively hypersecretes one or more hormones (Metz and Jensen, 2008; Oberg and Eriksson, 2005), further burdening the ER. For example, while each normal pancreatic β-cell is capable of releasing an estimated 1 million molecules of insulin per minute (63), some “insulinoma” PanNET cells secrete over 10-fold higher amounts of this hormone even under hypoglycemic conditions (Scheuner and Kaufman, 2008). Clinically, these PanNETs are categorized as “functioning” because they secrete hormones that cause visible symptoms. It is important to note, however that even clinically silent “nonfunctioning” PanNETs usually secrete high levels of multiple hormones and peptides (e.g., CgA, synaptophysin) that do not cause clinical symptoms, allowing these tumors to remain undetected until late stage. For example, elevated plasma levels of CgA are present in 60-100% of patients with nonfunctioning PanNETs and can be used

to follow disease progression, response to therapy, and relapse (66-68). Thus, although these PanNETs are characterized as “nonfunctioning” and are clinically undetectable, they still have abnormally high secretory demands. Prior to this, however, there were no formal studies investigating the ER stress and UPR activation status of PanNETs. We predicted that PanNETs, which have uncontrolled protein secretion and are subject to other ER stress insults *in vivo* (e.g., hypoxia), are even more dependent on the UPR than their healthy endocrine cell counterparts and that, if this proved to be true, targeting the UPR could be an effective strategy against PanNETs and other secretory cancers.

Although we hypothesized that UPR signaling may benefit secretory cancers such as PanNETs, the role of the UPR in cancers has been controversial, as described above. For example, inactivating somatic mutations in IRE1α were discovered in human glioblastoma (S769F) and ovarian serous carcinoma (P830L), which is inconsistent with the notion that the UPR is beneficial to tumor survival and growth (Ghosh et al., 2014; Greenman et al., 2007). We sought to clarify this by analyzing the signaling outputs of the UPR.

Indeed, we present evidence here of UPR hyperactivation, including the IRE1α/XBP1s axis, in human PanNET samples and INS-1 xenografts. The signaling outputs of the UPR in these tumor cells seem to be carefully balanced and biased towards adaptation.

Results

Primary Human PanNETs and a Xenograft PanNET Model Both Show Evidence of ER Stress

To look for markers of ER stress and UPR activation, we performed immuno-histochemistry (IHC) against the ER chaperone BiP/GRP78, which is upregulated by the adaptive UPR when misfolded proteins accumulate in the ER, on a panel of six human PanNETs obtained from the UCSF Department of Pathology. The expression of BiP/GRP78 was markedly higher in 5 of the 6 human PanNETs compared with normal pancreas (Fig 3B-C, Supplemental Fig 1), indicating an elevated level of protein-folding stress in these tumors. Moreover, we found that *XBP1* splicing (a readout for IRE1α signaling) and *ATF4* mRNA expression (a readout for PERK signaling) were both strongly upregulated in human PanNETs compared with normal pancreas (Fig 3D-E).

Based on these data, we hypothesized that PanNETs may require an elevated level of adaptive UPR signaling to accommodate their high protein-folding demands and avoid ER stress-induced apoptosis. Therefore, we set up a PanNET xenograft mouse model in which to carefully study the growth of tumors *in vivo*. Rat insulinoma (INS-1) cells are one of the most widely used PanNET lines because they secrete insulin in response to glucose and have previously been used in xenograft studies (Asfari et al., 1992; Babu et al., 2013). We injected 5 million INS-1 cells subcutaneously (s.c.) into the flanks of immunodeficient NOD-*scid* IL2Rgamma^{null} (NSG) mice (Fig 3F). Tumors became palpable at 1-2 weeks post-injection and closely resembled human PanNETs by

histology and IHC staining for known markers, including insulin, chromogranin A (CgA), and synaptophysin (SPH) (Fig 3G-J). Moreover, CD31 staining demonstrated that the INS-1 xenografts showed similar vascular patterns compared with human PanNETs (Fig 3K). Notably, similar to human PanNETs, INS-1 xenograft tumors showed evidence of increased ER stress (Bip/GRP78) and upregulated IRE1α signaling (*Xbp1* splicing) compared with the same INS-1 cells grown *in vitro* (Fig 3L-M).

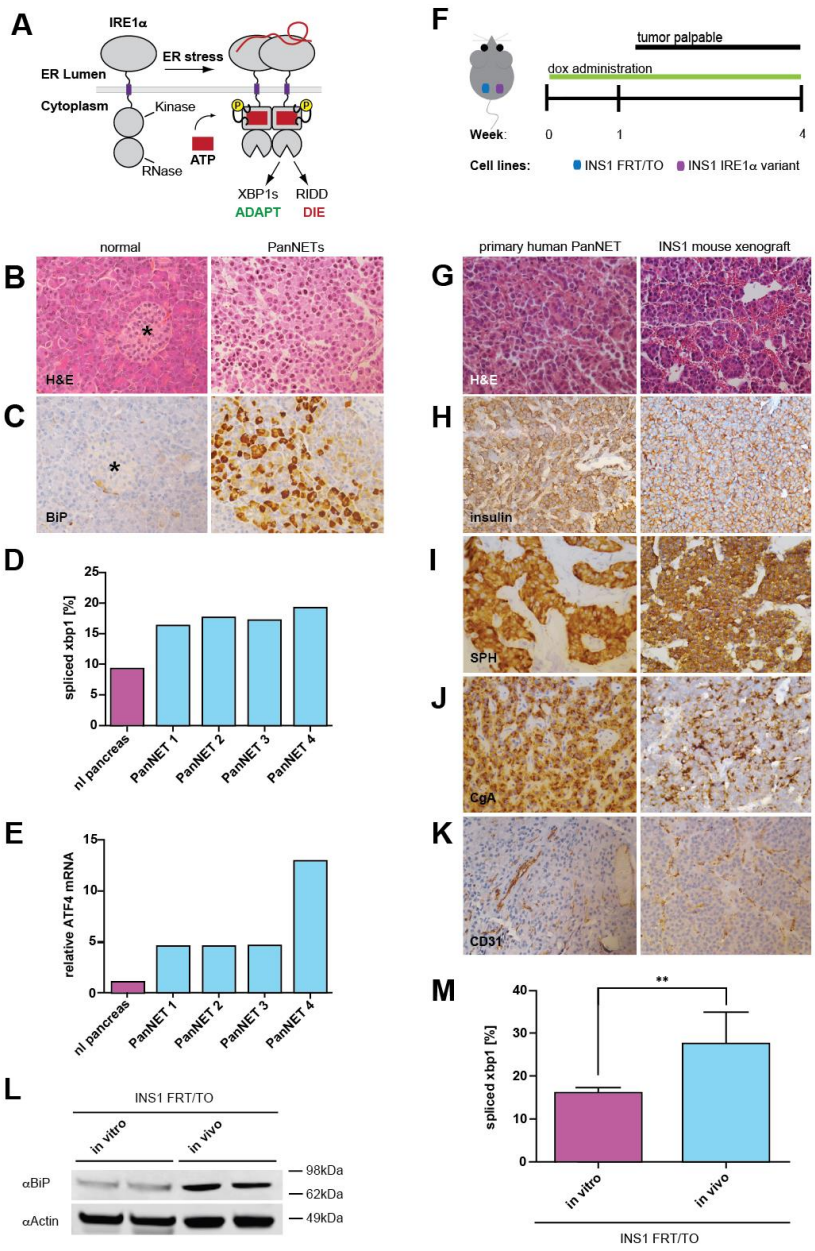

Figure 3. PanNETs show evidence of ER stress and UPR activation.

A. Simplified model of IRE1α signaling. In response to an accumulation of ER misfolded proteins, the bifunctional IRE1α kinase/RNase dimerizes/tetramerizes to cleave a non-conventional intron from XBP1 mRNA, which upon re-ligation encodes the XBP1s transcription that upregulates ER protein-folding and quality control components to promote adaptation. However, if hyperactivated by sustained ER stress, IRE1α oligomerizes and its relaxed RNase activity endonucleolytically degrades many mRNAs—a process called regulated IRE1α-dependent decay (RIDD)--at the ER membrane to cause cell death. B. H&E and C. BiP/GRP78 IHC on representative normal pancreas and primary human PanNET. Star indicates islet of Langerhans. D. Percent *xbp1* splicing and E. relative *ATF4* mRNA expression from 4 primary human PanNETs and normal pancreas. F. PanNET xenograft experimental setup. 5 million INS-1 cells (FRT/TO control vs INS-1 variant) injected s.c. in bilateral flanks of NSG mice. FRT/TO tumors become palpable by ~10 days and mice are sacrificed for tumor endpoint at 4 weeks post-injection. G-K. Mouse INS-1 xenografts and human PanNETs have similar morphology and staining for classic PanNET markers. CgA=chromogranin A, SPH=synaptophysin. 40x magnification. L. Immunoblot shows higher BiP/GRP78 in INS FRT/TO xenograft tumors 4 weeks post-injection compared with INS-1 FRT/TO cells grown in culture, indicating higher overall ER stress *in vivo*. M. Increased spliced *xbp1* in INS FRT/TO xenograft tumors 4 weeks post-injection compared with INS-1 FRT/TO cells grown in culture, indicating increased activation of IRE1α *in vivo*. Error bars represent 1 SD of the mean from 7 *in vitro* and 14 *in vivo* samples. p=0.0016. (*<.05, **<.01, ***<.001, ****<.0001)

IRE1α Cancer Mutants Promote INS-1 Tumor Growth

Previously, we engineered multiple transgenic INS-1 cell lines that express Tet repressor and are stably integrated with Doxycycline (Dox)-inducible constructs driving various IRE1α mutants (Fig 4) (Han et al., 2009; Shuda et al., 2003). Addition of Dox leads to overproduction of transgenic IRE1α proteins, which causes IRE1α to spontaneously oligomerize and trans-autophosphorylate by mass action, activating the RNase to induce *Xbp1* splicing, ER-localized mRNA decay, and a Terminal UPR (Han et al., 2009). Therefore, we used this system to forcibly express IRE1α variants in INS-1 cells *in vivo* by feeding the mice Dox chow (transgene ON).

To test whether upregulation of IRE1α's adaptive signaling could promote tumor growth, we expressed two cancer-associated IRE1α mutants in our xenograft system. These somatic mutations in IRE1α were discovered in human glioblastoma (S769F) and ovarian serous carcinoma (P830L), and we have found that they partially cripple the protein such that IRE1α is only capable of signaling adaptation and is defective in triggering apoptosis (Ghosh et al., 2014; Greenman et al., 2007) (Figure 4A). In contrast to INS-1 FRT/TO cells, Dox administration to overexpress INS-1 IRE1α(S769F) or INS-1 IRE1α(P830L) leads to a significant increase in tumor size (Fig 4B-D), suggesting that these two cancer mutants can indeed promote tumor growth.

Moreover, Dox-induction of IRE1α P830L and IRE1α S769F led to small increases in *Xbp1* splicing (Figure 4E), but dramatic decreases in RIDD as measured by *Ins-1* decay (Figure 4F), such that these mutants appear to serve as dominant negatives against

apoptotic signaling downstream of IRE1α. Hence, these data suggest that altering the balance of IRE1α's adaptive vs. apoptotic signaling can have major consequences on tumor growth.

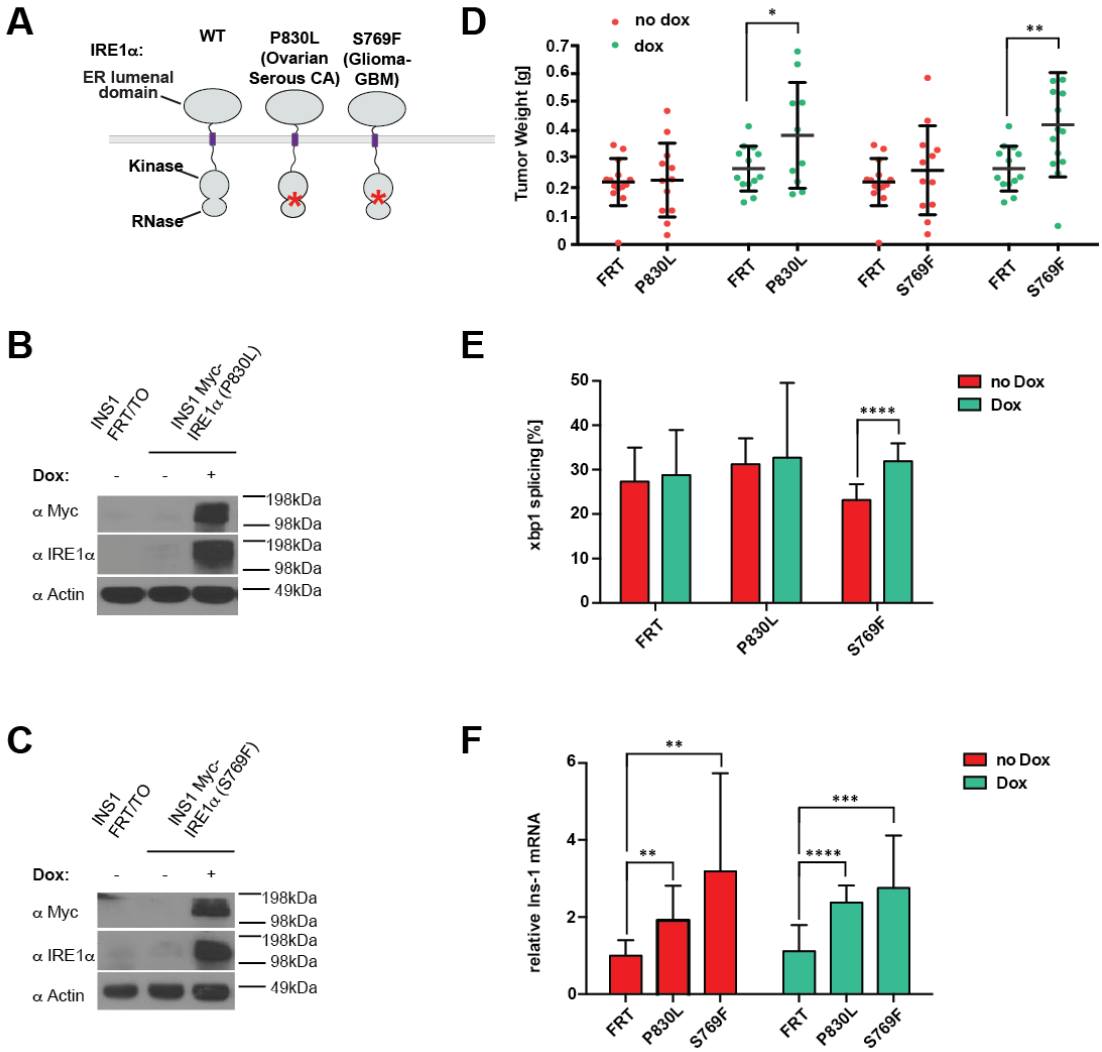

Figure 4. IRE1α mutations found in human cancers cause an imbalance in adaptive and apoptotic signaling.
A. IRE1α is a transmembrane protein with an ER lumenal domain and cytoplasmic kinase and RNAse domains. The mutants used have mutations in the kinase domain or the linker region between the kinase and RNase domains. Star indicates mutation site. B. Comparison of tumor weights with and without transgene expression, induced by administration of Doxycycline chow (green). Error bars represent 1 SD of the mean from >10 samples as follows: n(FRT)=14, n(P830L)=12, p=0.019; n(FRT)=14, n(S796F)=12 tumors, p=0.0038. C. Immunoblot showing Myc and IRE1α expression in INS-1 FRT/TO and INS-1 IRE1α(P830L) tumors at 4 weeks post-injection. D. Immunoblot showing Myc and IRE1α expression in INS-1 FRT/TO and INS-1 IRE1α(S796F) tumors at 4 weeks post-injection. E. Percent spliced *xbp1* with and without Dox-induced transgene expression. p<0.0001. F. Relative insulin mRNA. FRT vs P830L (no Dox) p=0.0020; FRT vs S796F (no Dox) p=0.0029; FRT vs P830L (Dox) p<0.0001; FRT vs S796F (Dox) p=0.0003.

Discussion

Normal pancreatic neuroendocrine cells are critically dependent on the UPR for proper development and maintenance, an observation that we find to translate to PanNETs. While healthy endocrine cells secrete large amounts of protein in response to appropriate signals, PanNETs constitutively hypersecrete one or more hormones, further burdening an already-burdened ER. Clinically, PanNETs are categorized as "functioning" only if they secrete hormones that cause visible symptoms (Baudin et al., 1998; Nobels et al., 1998; Pirker et al., 1998). It is important to note, however that even clinically silent "nonfunctioning" PanNETs usually secrete high levels of multiple hormones and peptides (e.g., CgA, synaptophysin) that do not cause clinical symptoms, allowing these tumors to remain undetected until late stage. Thus, although these PanNETs are characterized as "nonfunctioning," they still have abnormally high secretory demands. Because of this, we predicted that PanNETs are even more dependent on the UPR than their healthy endocrine cell counterparts, and indeed, we present evidence here of UPR hyperactivation, including the IRE1α/XBP1s axis, in both human PanNET samples and INS-1 xenografts. Notably, in our panel of human PanNETs, one sample did not express insulin by IHC, but it did express CgA, SPH, and elevated BiP (Supplemental Figure 1).

We hypothesized that PanNETs may experience elevated ER stress and therefore be particularly sensitive to imbalances in UPR signaling, but it was initially unclear how the UPR might contribute to tumor survival and growth. Many studies have shown evidence of sustained and high level UPR activation in various cancers, including myeloma,

glioblastoma, and carcinomas of the breast, stomach, esophagus, and liver (Carrasco et al., 2007; Chen et al., 2002; Fernandez et al., 2000; Gardner and Walter, 2011; Shuda et al., 2003; Song et al., 2001), but most of the rare cases of somatic mutations in UPR components have been loss of function (31). Some studies have shown that XBP1s and PERK promote tumor progression (32, 33), arguing that UPR signaling may be beneficial for tumor survival. Hence, whether the UPR ultimately inhibits or promotes solid tumor growth in patients has remained an area of intense debate (33-38).

The signaling outputs of the UPR in PanNET cells seem to be carefully balanced and biased towards adaptation. In this model, we expressed cancer-associated mutations in IRE1α and found that they serve as dominant negatives and selectively disable the apoptotic outputs of IRE1α while maintaining its homeostatic outputs. This does not clarify whether the UPR is pro- or anti-tumorigenic overall. If anything, this suggests that the former question is insufficiently nuanced and that tumors depend on a certain balance of Adaptive vs. Terminal UPR signals. An increase in Adaptive UPR signals such as XBP1s are beneficial to tumors, but the cells must find a way to ensure that they Adaptive UPR signals are not elevated at the expense of triggering the Terminal UPR. At least some cancer cells appear to evolve mechanisms to increase the ratio of the Adaptive/Terminal UPR to enhance survival.

Chapter 2: IRE1α signaling must be tightly titrated in PanNETs

Introduction

IRE1α is a critical life-death switch under conditions of ER stress. IRE1α contains an ER lumenal domain that directly binds unfolded proteins and dimerizes in response (Aragon et al., 2008, 2009; Credle et al., 2005; Zhou et al., 2006). On the cytosolic side, IRE1α has two distinct enzymatic domains—a kinase and RNase. Modulation of the auto-phosphorylation status of its kinase allosterically controls the activity and substrate specificity of the adjacent RNase domain to determine cell fate under ER stress (Han et al., 2009). Remediable ER stress restricts IRE1α enzymatic activity to a single adaptive substrate, the homeostatic transcription factor XBP1s (s=spliced), which upregulates genes encoding ER protein-folding and quality control components, such as BiP/GRP78, culminating in the "Adaptive UPR" (Lee et al., 2003).

Under conditions of irremediable ER stress (Figure 1B), sustained, high-level kinase autophosphorylation causes higher order IRE1α oligomerization and relaxed specificity of IRE1α's Rnase, allowing it to endonucleolytically degrade many mRNAs at the ER membrane that encode secretory proteins, such as insulin (Han et al., 2009; Hollien et al., 2009), as well as essential components of the ER protein-folding machinery. The net consequence of high-level IRE1α Rnase activation is that it promotes the deterioration of ER function. Moreover, hyperactivated IRE1α endonucleolytically degrades select microRNA precursors as a mechanism that upregulates key apoptotic signals, including Thioredoxin-Interacting Protein (TXNIP) (Lerner et al., 2012; Upton et al., 2012). Thus,

hyperactive IRE1α Rnase activity induces a "Terminal UPR," whereby adaptive signaling through *Xbp1* splicing is eclipsed by pro-apoptotic signals (Upton et al., 2012). These effects have been thoroughly investigated by our lab and others *in vitro*, and we predicated that we would observe similar effects *in vivo* in response to hyperactivation of WT IRE1α.

Conversely, little is known about the effects of inactivating or deleting IRE1α, which is a more therapeutically relevant and therefore more clinically interesting question. It is known, as previously described, that IRE1α is critical to development and that knocking out UPR components, including *Ire1α,* causes embryonic lethality. At best, islet cell-specific knockout of UPR components causes cell dysfunction and death, all of which suggests that these components are essential. Contrary to this notion, inhibition of IRE1α using a potent and selective kinase had little effect on many non-PanNET cancer cell lines *in vitro* (Amgen paper). Prior to this study, however, there had been no such temporally regulated studies *in vivo* or investigations of IRE1α modulation in PanNETs.

We hypothesized that because of the above-average ER stress and UPR activation in PanNETs, they would be critically dependent on a balance of Adaptive vs. Terminal IRE1α signals and that pushing the balance of IRE1α signaling in either direction (i.e. either increasing Terminal UPR signals to induce apoptosis or decreasing pro-survival Adaptive UPR signals) would be detrimental to the survival and growth of PanNETs.

Results

IRE1α Hyperactivation Triggers Apoptosis to Decrease INS-1 Tumor Burden

We next tested the effects of wild-type IRE1α hyperactivation on tumor growth and survival by injecting equal numbers of Dox-inducible INS-1 IRE1α(WT) and INS-1 FRT/TO (vector control) cells into the flanks of NSG mice. Dox chow alone had no effect on the size of INS-1 FRT/TO tumors over a 4-week time course. In contrast, Dox–induced expression and hyperactivation of IRE1α(WT) markedly reduced tumor size to barely 30% of INS-1 FRT tumors (Fig 5A-C). The reduction in INS-1 tumors upon IRE1α hyperactivation was associated with significant increases in both adaptive and apoptotic outputs (Fig 5D-F), and apoptosis as measured by TUNEL and cleaved Caspase-3 staining (Fig 5G-H; Supplemental Fig 4C-D). No significant changes in proliferation, as measured by Ki67 staining, were found (data not shown). This is consistent with observations *in vitro* that despite continued *Xbp1* splicing, the Terminal UPR eventually eclipses the survival benefits of these adaptive signals.

Interestingly, we noted that in the absence of Dox, tumors composed of INS-1 IRE1α(WT) cells were consistently larger than those composed of vector control INS-1 FRT/TO cells (Figure 5A). One likely explanation for this observation is that the IRE1α transgene construct was slightly leaky in the absence of Dox (Figure 5B-C), and this marginally elevated IRE1α expression promoted increased *XBP1* splicing without significantly increasing IRE1α's apoptotic outputs (Figure 5D-F), similar to the effect of the cancer mutants. This result further supports the idea that the balance of adaptive and apoptotic signals downstream of IRE1α is tightly titrated, and if altered impacts tumor growth and/or survival.

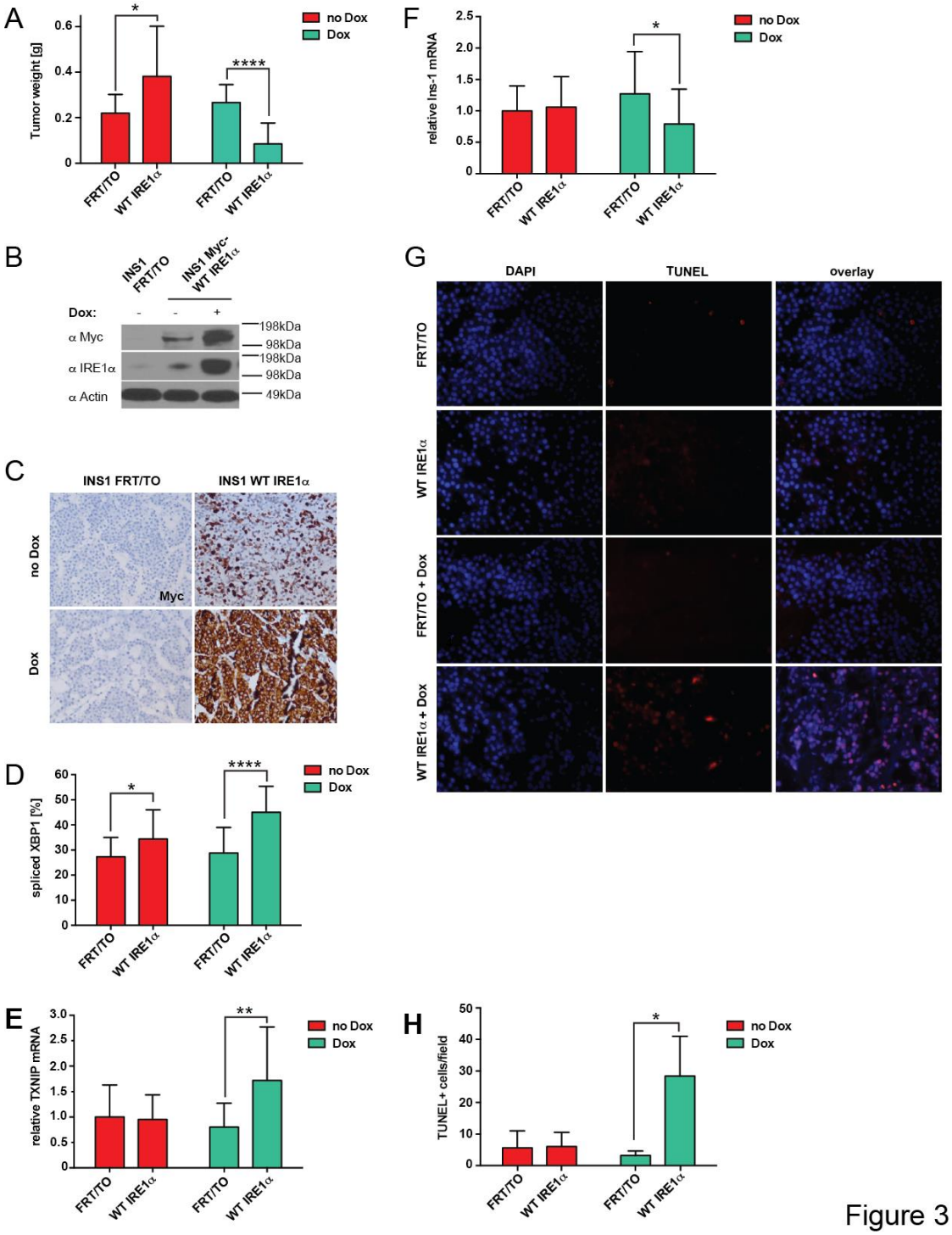

Figure 3

Figure 5. Hyperactivation of WT IRE1α leads to apoptosis.
A. Weights of INS-1 xenograft tumors at 4 weeks post-tumor cell injection. n(FRT no Dox)=14, n(WT no Dox)=20, n(FRT Dox)=13, n(WT Dox)=18. FRT vs WT (no Dox) p=0.045; FRT vs WT (Dox) p<0.0001. B. Immunoblot showing transgenic Myc-tagged IRE1α expression in tumors at 4 weeks post-injection. C. Representative images of Myc staining in INS-1 xenograft tumors at 4 weeks post-injection. D. Percent spliced *xbp1* in INS-1 xenograft tumors at 4 weeks post-injection. FRT vs WT no Dox: p=0.048; FRT vs. WT Dox: p<0.0001. E. Relative *TXNIP* mRNA levels in INS-1 xenograft tumors at 4 weeks post-injection. p=0.005. F. Relative *Ins-1* mRNA levels in INS-1 xenograft tumors at 4 weeks post-injection. p=0.05. G. Representative images of tumors stained for TUNEL and DAPI. Blue=DAPI. Red=TUNEL. H. Quantification of TUNEL staining in numbers of TUNEL-positive cells per field. 4-5 samples were stained per group, and at least 5 high-powered fields (40x magnification) were imaged per sample. p=0.012.

CRISPR/Cas9-directed inactivation of *Ire1α* or *Xbp1* cripples INS-1 tumor growth

In order to test the effects of disrupting the IRE1α axis on INS-1 tumors, we first used the CRISPR/Cas9 gene editing system to functionally inactivate either *Ire1α* or its primary adaptive target, *Xbp1,* in the INS-1 FRT/TO parental line (Fig 6A, E). Successful IRE1α and XBP1s deletion was confirmed by immunoblot (Fig 6E). Spliced *Xbp1* was also completely eliminated when upstream IRE1α was removed (Fig 6A, D; Supplemental Fig 2A). In contrast, CRISPR/Cas9 editing of *Xbp1* introduced a stop site distal to its IRE1α cleavage site, such that *Xbp1* mRNA splicing continues to occur, and, in fact, is increased due to IRE1α hyperactivation but fails to be translated into a functional transcription factor XBP1s.

While these INS-1 IRE1α KO and INS-1 XBP1 KO cells grow at equivalent rates compared with parental INS-1 FRT/TO cells in culture for up to 6 days (Fig 6H), they both showed markedly reduced tumor growth *in vivo*, exhibiting a lower ratio of Ki67-positive cells (Fig 6I-J) and barely attaining 10% of the weight of control INS-1 FRT/TO tumors (Fig 6B-C, F-G). Importantly, INS-1 FRT/TO cells subjected to a non-targeting CRISPR/Cas9 control achieved a similar tumor weight as that of the parental FRT/TO INS-1 cells *in vivo* (Supplemental Fig 3B). Interestingly, the INS-1 XBP1 KO tumors exhibited increased *Ire1α* and *Xbp1* mRNA expression (Supplemental Fig 2C-D), suggesting that the loss of this adaptive transcription factor leads to increased ER stress and thwarted attempts to activate adaptive UPR signaling. Together, these data demonstrate that despite no obvious differences in cell behavior *in vitro*, *in vivo*

PanNETs are critically dependent on the adaptive outputs of IRE1α for growth and survival.

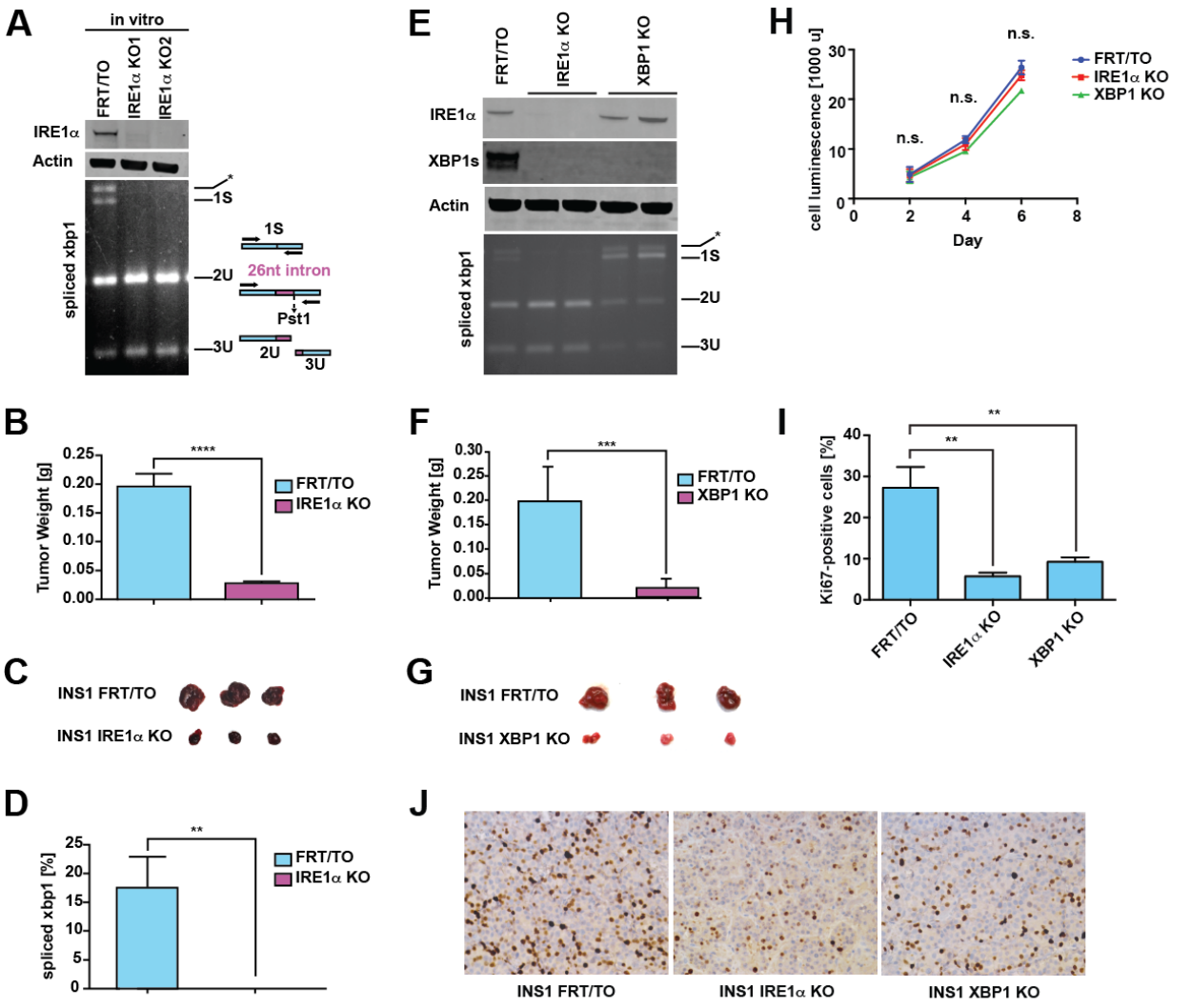

Figure 6. CRISPR/Cas9-mediated deletion of *Ire1α* and *Xbp1s* in INS-1 tumors dramatically decreases tumor burden.
A. Top: Immunoblot showing IRE1α expression in INS-1 IRE1α KO cells compared with INS-1 FRT/TO cells *in vitro*. Actin was used as a control. Bottom: Gel showing *xbp1* splicing (second band from the top) with a diagram of the assay to the right. B. Weights of INS-1 FRT/TO tumors compared with INS-1 IRE1α KO tumors at 4 weeks post-injection. n=20 per group, p<0.0001. C. Photo of 3 representative INS-1 FRT/TO and 3 representative INS-1 IRE1α KO tumors at 4 weeks post-injection. D. Quantification of spliced *Xbp1* in INS-1 FRT/TO vs INS-1 IRE1α KO tumors at 4 weeks post-injection. n=3 per group, p=0.030. E. Immunoblot showing IRE1α and XBP1 expression in INS-1 IRE1α KO and INS-1 XBP1 KO cells. F. Weights of INS-1 FRT/TO tumors compared with INS-1 XBP1 KO tumors at 4 weeks post-injection. n=6 per group, p=0.0021. G. Photo of 3 representative INS-1 FRT/TO and 3 representative INS-1 IRE1α KO tumors at 4 weeks post-injection. H. Cell proliferation *in vitro*, as measured by the Cell Titer Glo assay, where cell luminescence is a measurement of cell metabolic activity. Cells were measured at 2, 4, and 6 days after seeding in a 96-well plate. n.s.=not significant. I. Percent Ki67-positive cells in tumors at 4 weeks post-injection. IRE1α KO: n(FRT)=5, n(KO)=5, p=0.0030; XBP1 KO: n(FRT)=5, n(KO)=4, p=0.0042. J. Representative images of Ki67 staining in tumors at 4 weeks post-injection.

Discussion

Because PanNETs experience higher-than-normal levels of ER stress and UPR activation, we predicted that PanNETs would also be sensitive to the loss of these pro-homeostatic signals downstream of IRE1α. When CRISPR/Cas9 was used to genetically inactivate *Ire1α* or *Xbp1,* the decrease in tumor burden compared with INS-1 FRT/TO control tumors was dramatic. Importantly, while we observe no significant difference in rates of cell proliferation *in vitro,* INS-1 IRE1α KO and INS-1 XBP1 KO tumors are much less proliferative (Ki67 staining) than the parental lines or CRISPR/Cas-9 non-targeting controls. This reinforces the importance of our early observation that the INS-1 FRT tumors experience elevated ER stress and UPR activation *in vivo* versus *in vitro*, and that cells are critically reliant on the IRE1α/XBP1 arm only when they encounter stressful micro-environmental conditions. In culture, given all necessary nutrients, INS-1 cells do not need to activate IRE1α or downstream XBP1s, so deletion of these UPR components does not hinder their survival. In a tumor, however, these same INS-1 cells may experience greater hypoxia (particularly in the center of the tumor mass), ER stress, glucose deprivation, and other environmental stresses commonly found in solid tumors. Faced with these stresses, they need a robust and active UPR, and the absence of IRE1α and adaptive XBP1s becomes a hindrance to their ability to thrive. We also find that *Ire1α* levels are elevated in INS-1 XBP1 KO tumors, reflecting efforts to respond to heightened ER stress and echoing previous findings that IRE1α activity increased in normal pancreatic β-cells in response to *Xbp1* deletion.

Chapter 3: A monoselective IRE1α inhibitor decreases tumor burden in two preclinical mouse models

Introduction

Our team developed first-in-class ATP-competitive IRE1α *K*inase *I*nhibiting *R*Nase *A*ttenuators—*KIRAs*—that bind IRE1α's kinase domain and allosterically inhibit its RNase (Ghosh et al., 2014). Recently a more potent and selective KIRA series was published; when administered to a large panel of cultured non-PanNET tumor cell lines for 48h, these KIRAs had no effect on cell viability (Harrington et al., 2015). This result is consistent with our findings that IRE1α activity is relatively low in cultured cells, and that INS-1 IRE1α KO and INS-1 XBP1 KO cells grow equivalently to INS-1 FRT/TO cells *in vitro* (Fig 6).

Results

A monoselective IRE1α kinase inhibitor promotes INS-1 cell cycle arrest and apoptosis *in vivo* and decreases tumor burden

We re-synthesized a monoselective IRE1α inhibitor from this series (compound 18), which has recently been renamed KIRA8 (Fig. 7A) (Morita S, et al. Cell Metabolism, 2017;25:883-7). Not only did KIRA8 fail to inhibit any of the other >100 kinases tested *in vitro* (Harrington et al.), it is so selective against IRE1α that it even has minimal inhibition against the closely related paralog, IRE1β (Morita, S, et al). Pharmacokinetic studies in mice showed that daily intraperitoneal (i.p.) dosing (50mg/kg) of KIRA8 is sufficient to provide plasma levels above its IC50 for RNase inhibition. C57BL/6 and

NSG mice treated with 50mg/kg daily i.p. dosing of KIRA8 for up to 1 month resulted in no change in body weight, complete blood count, or other obvious toxicities (data not shown). Moreover, as opposed to PERK inhibitors, which cause pancreatic b-cell toxicity, first generation KIRA6 and second generation KIRA8 have been shown to have significant β-cell sparing effects in multiple diabetes models (Ghosh Cell paper: Morita S, et al. Cell Metabolism, 2017;25:883-7). Hence, KIRA8 is an ideal tool compound to test the effects of pharmacologically inhibiting IRE1α *in vivo.*

Similar to *Ire1α* deletion, and consistent with its failure to induce toxicity in other cultured cancer cell lines (Harrington PE et al), KIRA8 administration at doses sufficient to essentially eliminate XBP1 mRNA splicing had no noticeable effects on growth rate or apoptosis of INS-1 FRT/TO cells for up to 5 days in culture (Fig 7B-C). While less dramatic than CRISPR/Cas9-directed inactivation of *Ire1α*, KIRA8 administration at 50mg/kg significantly reduced *Xbp1* splicing in the INS-1 FRT/TO tumors to ~50% of that in vehicle-treated tumors (Fig 7F-G), confirming IRE1α inhibition *in vivo*. Moreover, in sharp contrast to its lack of effect on INS-1 FRT/TO cell growth *in vitro*, KIRA8 administration *in vivo* for 3 weeks led to significantly smaller tumors (Fig 7D-E), a finding that phenocopies the INS-1 IRE1α KO and INS-1 XBP1 KO tumors.

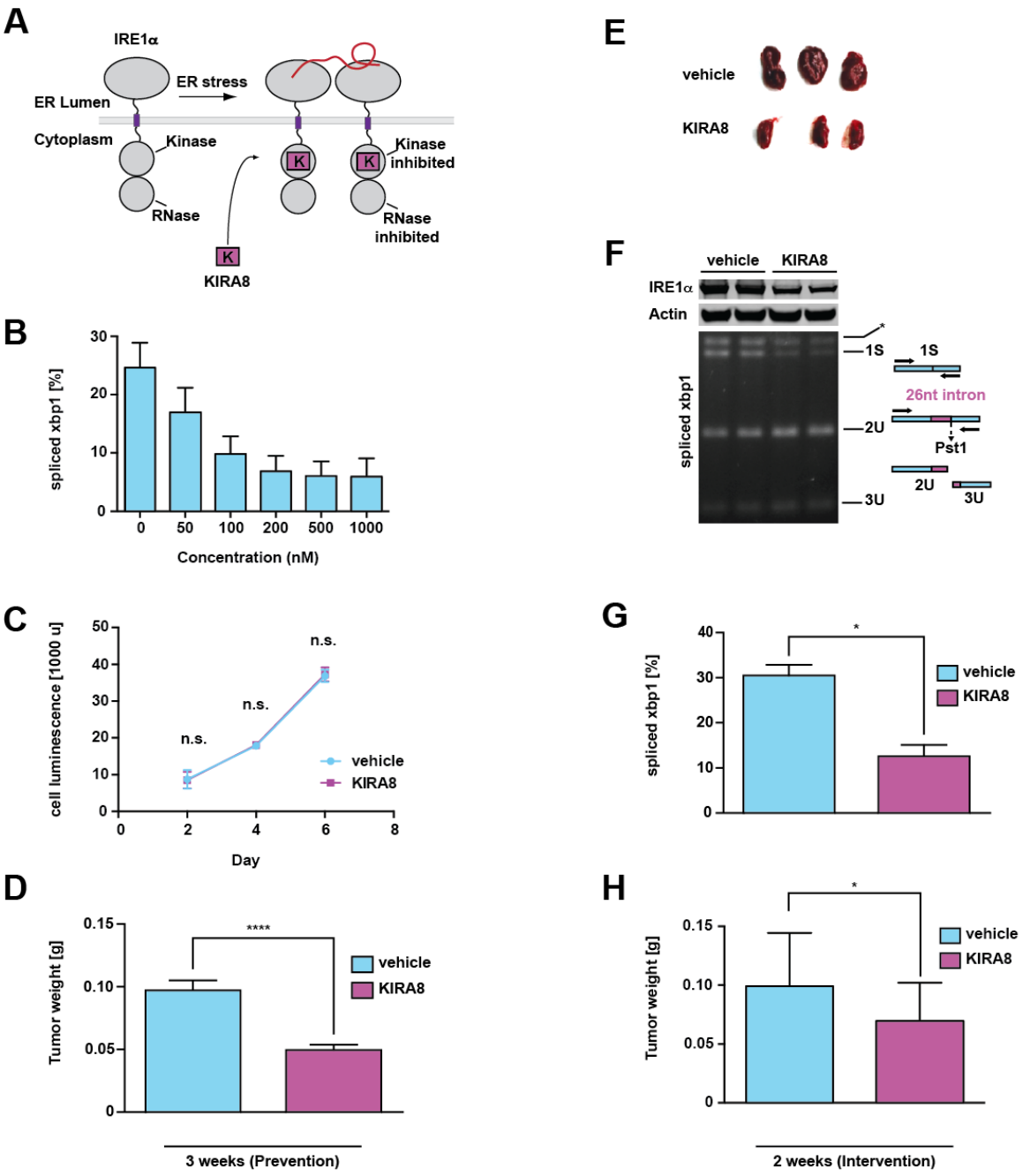

Figure 7. KIRA8 treatment has no effect on INS-1 cells *in vitro* but significantly decreases tumor burden *in vivo*.
A. KIRA8 is a *K*inase *I*nhibiting *R*Nase *A*ttenuator, a small molecule that binds to the IRE1α kinase domain and allosterically inhibits the function of its RNase, preventing it from responding to ER stress in the cell. B. Percent spliced *Xbp1* in INS-1 FRT/TO cells treated with KIRA8 at specified concentrations for 5 days *in vitro*. C. Cell luminescence as a measure of cell proliferation, measured after 2, 4, and 6 days of KIRA8 treatment of INS-1 FRT/TO cells. D. Weight of INS-1 FRT/TO xenograft tumors after 3 weeks of treating animals with vehicle control or KIRA8. Treatment began 1 day after tumor cell injection. n=20 per group, p<0.0001. E. Representative images of INS-1 FRT/TO xenograft tumors after 3 weeks of treatment with either vehicle or KIRA8. F. Top: Immunoblot showing IRE1α expression in KIRA8-treated INS-1 FRT/TO tumors compared with vehicle-treated INS-1 FRT/TO tumors *in vivo*. Actin was used as a loading control. Bottom: Gel showing *xbp1* splicing (second band from the top) with a diagram of the assay to the right. G. Percent spliced *Xbp1* in INS-1 FRT/TO tumors treated for 3 weeks with either vehicle or KIRA8. n=6 per group, p=0.015 H. Weight of INS-1 FRT/TO xenograft tumors after 2 weeks of vehicle or KIRA8 administration, beginning at 2 weeks post-tumor cell injection. n=10 per group, p=0.025.

Importantly, we also investigated the effects of KIRA8 intervention on established tumors. We first injected INS-1 FRT/TO into NSG mice and allowed them to form tumors for 2 weeks before initiating KIRA8 for 14 days, a scenario that better represents the clinical situation where a patient would begin receiving the drug after diagnosis of existing tumors. Treating tumors with KIRA8 at this later stage of growth also led to a significant decrease in tumor burden compared with vehicle-treated tumors (Fig 7H).

INS-1 FRT/TO tumors exhibited markedly decreased Ki67 staining (Fig 8A-B) and contemporaneous upregulation of the cell cycle inhibitor p21 within 24h of KIRA8 administration (Fig 8E). More importantly, KIRA8 not only decreases cell proliferation, but also actively promotes apoptosis, as demonstrated by increased cleaved Caspase 3 and TUNEL staining within 24h of administration (Fig 8C-D, Supplemental Fig 5). This cytotoxicity was associated with increased ER stress (BiP/GRP78) and transcriptional and translational upregulation of pro-apoptotic factors such as *Txnip* and BIM (Fig 8F-G). Interestingly, KIRA8-treated tumors also showed signs of nutrient deprivation, demonstrated by increases in *Vegf-a, Hif1a, Glut1,* and *Glut2* mRNA (Fig 8H). All major tissues, including pancreas, from these animals were fixed and stained to look for microscopic evidence of toxicity, but no adverse effects were observed (data not shown). KIRA8 had no obvious effect on blood insulin levels (data not shown).

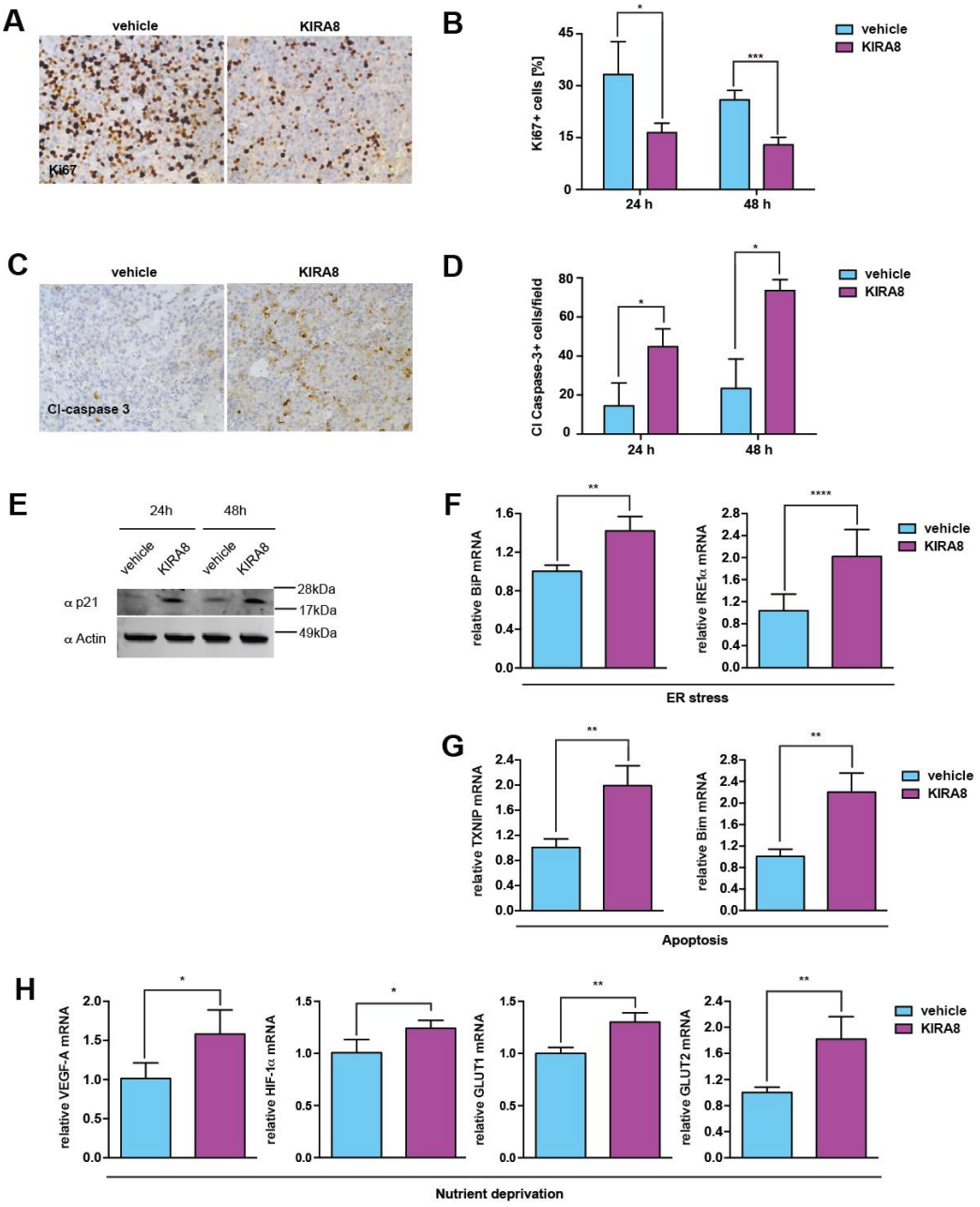

Figure 8. KIRA8 treatment is associated with increased cell cycle arrest and apoptosis and heightened ER stress and nutrient deprivation. A. Representative images of Ki67 staining in INS-1 FRT/TO tumors from mice treated with either vehicle control or KIRA8 for 24h, starting at 2 weeks post-tumor cell injection. 40x magnification. B. Quantification of Ki67-positive cells from INS-1 FRT/TO tumors treated with either vehicle control or KIRA8 for 24h and 48h. n=4 samples for each group, and at least 5 high-powered (40x) fields were imaged per sample. p(24h)=0.014, p(48h)=0.0003. C. Representative images of Cleaved Caspase-3 staining in INS-1 FRT/TO tumors from mice treated with either vehicle control or KIRA8 for 24h, starting at 2 weeks post-tumor cell injection. 40x magnification. D. Quantification of Cleaved Caspase-3-positive cells from INS-1 FRT/TO tumors treated with either vehicle control or KIRA8 for 24h and 48h. For each group, n=3, and at least 5 high-powered (40x) fields were imaged per sample. p(24h)=0.045, p(48h)=0.023. E. Representative immunoblot showing p21 expression in INS-1 FRT/TO tumors treated with either vehicle control or KIRA8 for 24h and 48h. Actin was used as a control. F. Expression of ER stress markers. Relative *Bip* and *Ire1α* mRNA expression in INS-1 FRT/TO tumors treated with either vehicle or KIRA8 for 48h. *Bip*: n(vehicle)=3, n(KIRA8)=4, p=0.0040; *Ire1α*: n(vehicle)=8, n(KIRA8)=10, p=0.00020. G. Expression of apoptosis markers. Relative *Txnip* and *Bim* mRNA expression in INS-1 FRT/TO tumors treated with either vehicle or KIRA8 for 48h. *Txnip*: n(vehicle)=7, n(KIRA8)=10, p=0.0036; *Bim*: n(vehicle)=4, n(KIRA8)=4, p=0.0015. H. Expression of markers of nutrient deprivation. Relative *Vegf-a, Hif1α*, *Glut1* and *Glut2* mRNA expression in INS-1 FRT/TO tumors treated with either vehicle or KIRA8 for 48h. *Vegf-a*: n(vehicle)=4, n(KIRA8)=4, p=0.017; *Hif1α*: n(vehicle)=4, n(KIRA8)=4, p=0.026; *Glut1*: n(vehicle)=3, n(KIRA8)=4, p=0.0032; *Glut2*: n(vehicle)=3, n(KIRA8)=4, p=0.0034.

Pharmacologic inhibition of IRE1α dramatically decreases tumor burden in the RIP-Tag2 transgenic mouse model of PanNET

In light of the critical role of IRE1α/XBP1 pathway for tumor growth in the INS-1 xenograft model, we decided to test the effects of KIRA8 in a second preclinical model of PanNET. The RIP-Tag2 mouse is a transgenic strain in which viral SV40 large T-antigen (Tag) expression is driven by rat insulin promoter-1 (RIP) (Hanahan, 1985), and this model has been extensively used as a model of endogenous pancreatic neuroendocrine tumorigenesis due to beta-cell specific expression of the Tag oncogene. These mice predictably develop islet hyperplasia (5-10wks), adenomas (10-12 wks), and eventually invasive and/or metastatic disease (13-15 wks) (Bergers et al., 1999). Moreover, the RIP-Tag2 model successfully predicted that sunitinib and everolimus would be effective in humans with advanced PanNET (Tuveson and Hanahan, 2011), which are now both FDA-approved for this indication. Hence, despite the artificial nature of the initial oncogenic event, the tumors in the RIP-Tag2 mouse seem to rely on some of the same signaling pathways as human PanNETs.

In order to best replicate clinical conditions, we performed a tumor regression trial; we began KIRA8 (50mg/kg daily i.p.) or vehicle administration at 12 weeks of age and continued therapy for 14 days. After the 2-week treatment period, we sacrificed the animals and fixed their pancreata for H&E and insulin staining to look for differences in tumor burden (Fig 9A). We also stained the tumor-free pancreata of age-matched wild-type C57BL/6 mice. Tumor burden was dramatically decreased in the KIRA8-treated mice compared with vehicle-treated control animals (Fig 9A-B). Based on these results,

we carried out a longer survival study following initiation of vehicle or KIRA8 treatment at 12 weeks of age. Impressively, while the vehicle-treated animals lived an average of 17 days after initiation of treatment, the KIRA8 animals survived over twice as long, with several animals surviving over 60 days (Fig 9C). We did not see signs of liver metastasis in either vehicle or KIRA8-treated mice (data not shown).

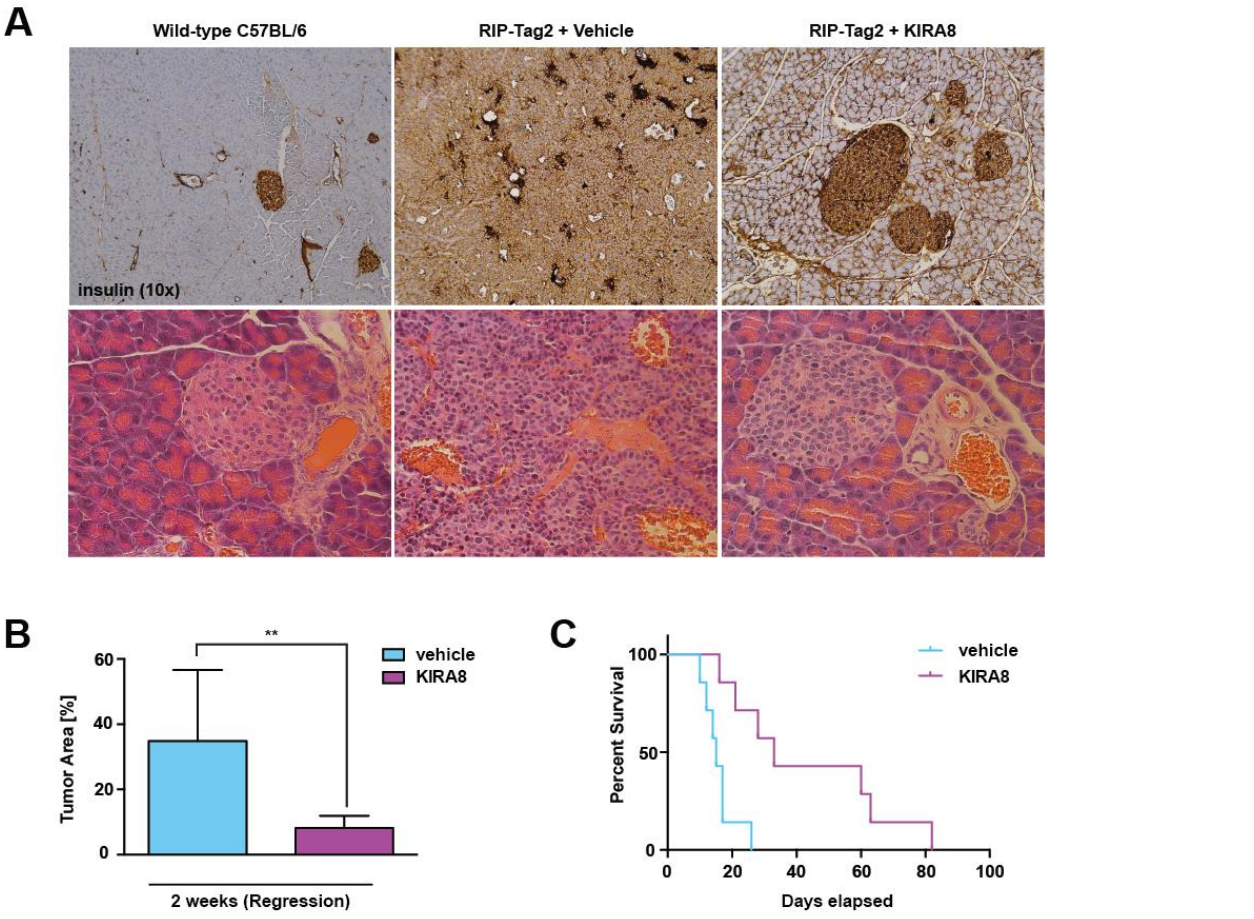

Figure 9. KIRA8 treatment decreases tumor size and prolongs survival of RIP-Tag2 animals.
A. Representative H&E on pancreata of wild-type C57BL/6 mice, RIP-Tag2 mice treated with vehicle, and RIP-Tag2 mice treated with KIRA8. B. Tumor area within representative pancreas H&E sections. n(vehicle)=7, n(KIRA8)=10, p=0.0015. C. Survival of RIP-Tag2 mice, where "Days elapsed" begins at time of injection at 12 weeks of age. n(vehicle)=7, n(KIRA8)=7, p=0.0033.

Discussion

Since the 1990s, the combination of streptozotocin, doxorubicin, and 5-fluorouracil has been the “gold standard” for advanced PanNETs (Moertel et al., 1980; Moertel et al., 1992). However, the 5-year survival for these patients is as low as 25% and a mere 4% for those with poorly differentiated tumors (Yao et al., 2008), and overall survival has not improved in >40 years (Halfdanarson et al., 2008a; Zhang et al., 2013). Treatment with targeted therapies, such as everolimus (an mTOR inhibitor) and sunitinib (a multi-kinase inhibitor), has prolonged progression-free survival of patients with metastatic PanNETs (Raymond et al., 2011; Yao et al., 2011), and both were FDA approved for this indication in 2011. However, the benefits of these targeted agents are relatively modest (~6 month increase in progression-free survival). Most recently, peptide receptor radiotherapy (PRRT), which uses radiolabeled somatostatin receptor (SSTR) ligands, has shown highly promising outcomes in clinical trials for some patients with metastatic SSTR-expressing PanNETs, but the fraction of patients who respond and the long term outcomes remain unknown (Cives and Strosberg, 2017). As such, there continues to be urgent need for greater insight into the molecular biology of PanNETs and the development of better therapies.

The promise of the dramatic results in INS1 “UPR KO” tumors prompted us to study the effects of chemical inhibition of IRE1α. KIRA8 was developed by Amgen, where the compound was tested on over 200 cancer cell lines, none of which were from PanNETs, for 48h. In that study, KIRA8 was found to have no effect on the viability of any of these cell lines in culture. However, as we have shown repeatedly, tumors confront hostile

microenvironmental conditions *in vivo* that are not adequately mimicked *in vitro*. We tested KIRA8 on cultured INS-1 cells at concentrations that essentially shut off IRE1α activity (as measured by *Xbp1* splicing) and also found negligible effects on growth and survival for up to 6 days, consistent with our observations of the INS-1 IRE1α and INS-1 XBP1 KO cells. However, a completely different story emerges *in vivo*. Within 24h, tumors from KIRA8-treated animals have reduced *Xbp1* splicing (confirming on-target activity), decreased proliferation as measured by Ki67, and cell cycle arrest as indicated by p21 upregulation. This is consistent with reports in pre-B acute lymphoblastic leukemia and other cancers that IRE1α inhibition and loss of *Xbp1s* leads to cell cycle arrest and cell death associated with increased p21 expression (Kharabi Masouleh et al., PNAS 2014; Sun et al, Oncotarget 2016). Moreover, after 24-48hr of KIRA8 treatment, the INS-1 tumors show upregulation of ER stress markers (Bip/GRP78), the apoptotic protein BIM, and begin undergoing apoptosis (Cleaved Casp3). This is consistent with findings in hematopoietic cells that *Xbp1s* has a direct anti-apoptotic effect, leading to decreases in pro-apoptotic *Bim* mRNA (Kurata 2011). Hence, pharmacologic inhibition of IRE1α *in vivo* leaves tumor cells without a strong adaptive response and leads to rapid growth arrest and apoptosis of INS-1 tumors.

When recipient mice are treated with KIRA8 for 3 weeks, their INS-1 tumors are about half the size of those of vehicle-treated animals. In sharp contrast to its lack of effect on INS-1 growth *in vitro*, KIRA8 administration results in significantly smaller tumors *in vivo*, a finding that phenocopies the INS-1 IRE1α KO cells grown *in vivo*. Not surprisingly, as KIRA8 administration resulted in only about a 50% decrease in IRE1α activity, as

measured by XBP1, the effects on tumor growth are not as pronounced as those of genetically deleting *Ire1*α, which completely eliminates XBP1 splicing. With more potent KIRAs, it should be possible to achieve greater anti-tumor effects. Notably, when we allow INS-1 tumors to grow for 2 weeks in the animals before beginning KIRA8 treatment, an experimental scheme that better mimics treatment of patients in the clinic, those tumors are also significantly smaller than tumors from vehicle-treated control animals. Importantly, no toxicity (including against normal islets) has been observed in tumor-bearing or healthy control mice for up to 2 months at the doses used.

Notably, the KIRA8-treated INS-1 tumors show upregulation of markers of hypoxic and ischemic stress, suggesting that the absence of adaptive IRE1α signaling to counteract these stresses render tumor cells even more vulnerable to a destructive ER stress-induced apoptotic cascade. We can mimic these conditions *in vitro* by using Tunicamycin (Tm) to induce ER stress and apoptosis in a dose-dependent manner. Apoptosis is intensified by the addition of KIRA8 to Tm-treated cells. Together, our results lead to a working mechanistic model in which tumor cell fate is critically dependent on the balance of Adaptive vs. Terminal IRE1α outputs to handle ER stress conditions, and KIRA8 treatment disrupts this balance by removing the primary adaptive output, XBP1s (Figure 8). Under normal conditions, INS-1 tumors experience ER stress and activate IRE1α, which in turn increases the production of Adaptive XBP1s. XBP1s is responsible for transcriptional activation of many genes encoding proteins that help restore ER homeostasis as well as repression of senescence and apoptosis-inducing *p21* and *Bim*. The introduction of KIRA8 under these conditions of ER stress blocks

IRE1α dimerization and phosphorylation, thus preventing activation of XBP1s. The failure to turn on Adaptive signaling further increases ER stress, as indicated by the increase in *Bip* and *Ire1α* mRNA, which triggers BIM-mediated mitochondrial apoptosis. Because IRE1α and therefore XBP1s are inhibited, the counterbalance against *Bim* and p21 upregulation is missing. It remains to be clarified what mediates the ER stress-induced increase in BIM. We have not observed consistent compensatory increases in other arms of the UPR but cannot completely rule them out. Little is known about ATF6, and there are comparatively few tools that can be used to study it. It is also possible that this apoptotic pathway is mediated by IRE1α itself. In addition to its key role as an RNase, IRE1α has also been shown to be a scaffold for proteins such as ABL and JNK, the latter of which has also been shown to be upstream of BIM (Morita Cell Metabolism 2017; Vandewynckel 2013). It is important to note that although KIRA8 potently inhibits the IRE1α kinase (and allosterically the RNase), thus shutting down its enzymatic activities, IRE1α is still present in the cell and able to serve as a scaffold, though relatively little is known about that role (Morita Cell Metabolism 2017).

Chapter 4: PERK has an important role in PanNET survival

Introduction

PERK is critical for beta cell survival and function

PanNETs originate from professional secretory cells, which are critically dependent on a functional UPR for proper development and maintenance. Homozygous deletion of *Perk* in mice causes massive and rapid β-cell apoptosis leading to infantile diabetes, pancreatic exocrine insufficiency, and early growth defects (53, 54). This phenocopies Wolcott-Rallison syndrome, a rare human diabetic syndrome caused by *PERK* mutations. This is consistent with the effects of deleting other UPR components.

Pharmacological modulators of PERK

GSK2656157, a highly selective ATP-competitive PERK inhibitor (Figure), has recently been developed and reported to have protective benefits in pre-clinical models of neurodegeneration (75). An earlier PERK inhibitor reduced growth of a human pancreatic adenocarcinoma xenograft model (99). Notably, PERK inhibitors show on-target toxicity resulting in pancreatic β-cell loss and hyperglycemia (75). Advanced PanNET is one clinical scenario where diabetes is considered an acceptable toxicity (as is the case for the FDA-approved drug Streptozotocin).

Results

CRISPR/Cas9-directed inactivation of *Perk* cripples INS-1 tumor growth

In order to test the effects of disrupting the PERK axis in INS-1 tumors, we used the CRISPR/Cas9 gene editing system to functionally inactivate *Perk* in the INS-1 FRT/TO parental line. Successful PERK deletion was confirmed by immunoblot against both total PERK and its activated phosphorylated form (Fig 10A, D). While these INS-1 PERK KO cells grow at equivalent rates compared with the parental INS-1 FRT/TO cells in culture for up to 6 days (data not shown), similar to the other UPR KO cells, they barely attain 10% of the weight of control INS-1 FRT/TO tumors (Fig 10B-C), similar to what was observed in INS-1 IRE1α KO and INS-1 XBP1 KO tumors.

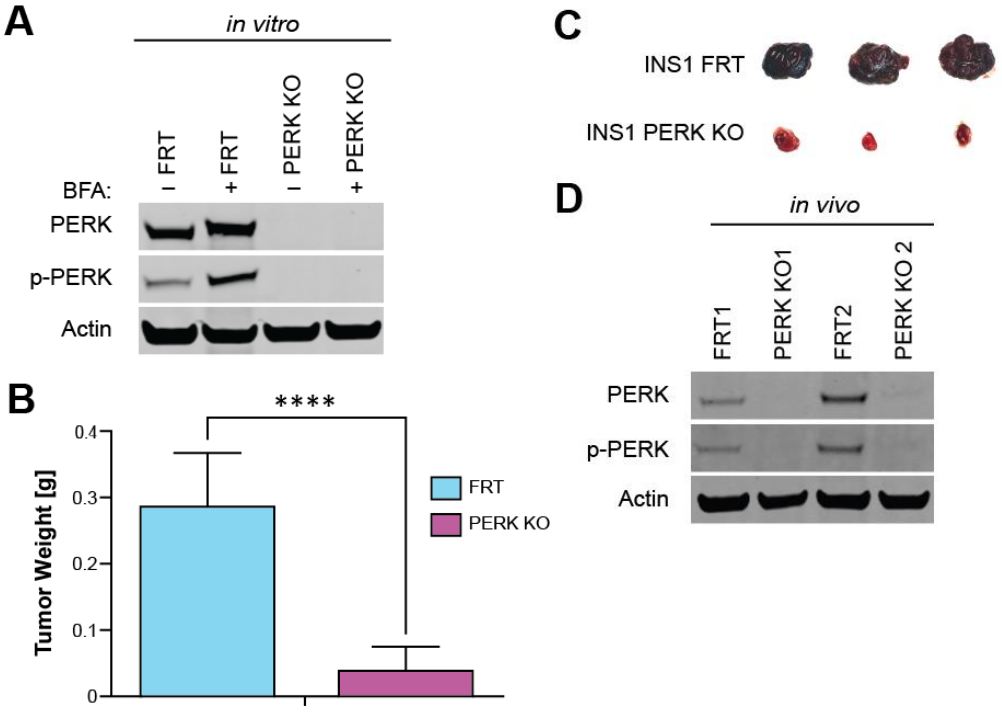

Figure 10. Genetic inactivation of PERK cripples tumor growth and decreases tumor burden. A. Immunoblot for PERK and p-PERK in INS-1 PERK KO cells compared with INS-1 FRT/TO cells *in vitro*. Actin was used as a loading control. BFA = brefeldin A, an ER stress agent that increases expression of both PERK and p-PERK. B. Weights of INS-1 FRT/TO and INS-1 PERK KO tumors. $p<0.0001$. C. Representative photos of INS-1 FRT/TO and INS-1 PERK KO tumors at 4 weeks post-INS-1 cell injection into NSG mice. D. Immunoblot for PERK and p-PERK in INS-1 FRT/TO and INS-1 PERK KO tumors at 4 weeks post-INS-1 cell injection.

A highly specific PERK kinase inhibitor decreases tumor burden in an INS-1 xenograft mouse model

GSK2656157, a highly selective ATP-competitive PERK inhibitor (Figure 11A), had similar antitumor effects in INS-1 FRT/TO tumors, decreasing PERK activation (Figure 11D) and tumor burden about 50% (Figure 11B-C).

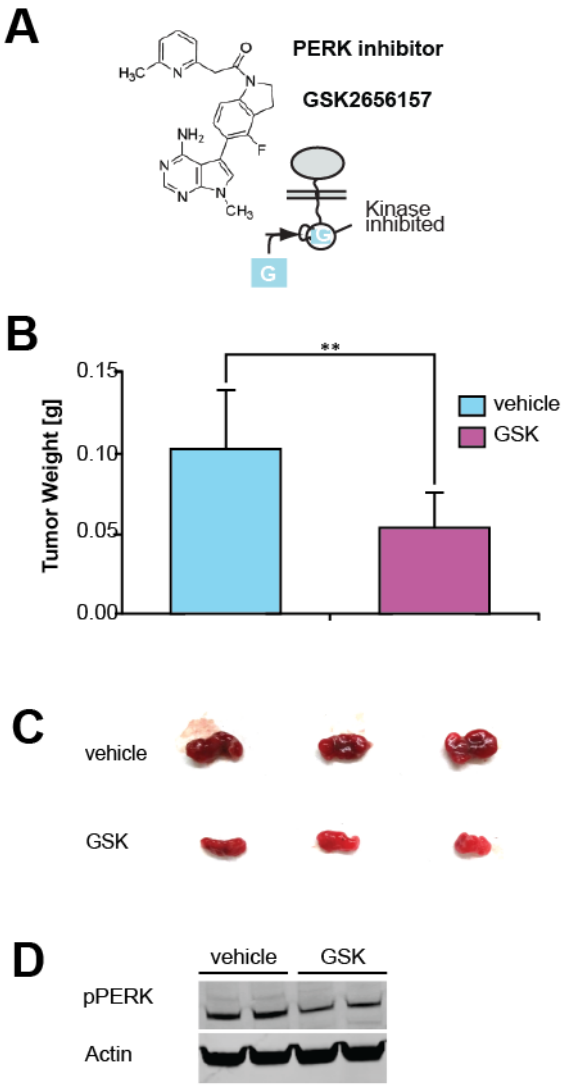

Figure 11. A highly selective PERK inhibitor decreases INS-1 tumor burden. A. GSK2656157 is a PERK kinase inhibitor. B. Weights of INS-1 FRT/TO tumors treated with either vehicle or GSK2656157 for 3 weeks by daily i.p. injection. p=0.001. C. Representative tumor photos. D. Immunoblot showing pPERK levels in vehicle and GSK2656157-treated INS-1 FRT/TO tumors. Actin was used as a loading control.

Discussion

PanNETs are known to arise sporadically or in association with familial cancer predisposition syndromes such as multiple endocrine neoplasia 1 (MEN1) (Halfdanarson et al., 2008b). Recent sequencing studies have found overlap in some genetic lesions that occur in sporadic and familial cases of PanNET. For example, 45% of sporadic PanNETs contain somatic mutations in the MEN1 tumor suppressor gene, and many of the remainder show loss of heterozygosity at this locus (Gortz et al., 1999; Reid et al., 2014; Scarpa et al., 2017). Additionally, nearly 15% of PanNETs have somatic mutations in one of several proteins in the mTOR (mammalian target of rapamycin) pathway (Gortz et al., 1999). Despite recent genetic insights, surgical resection is the only potentially curative treatment for PanNETs (Salaria and Shi, 2016). For the 20-30% of patients who have distant metastases at diagnosis, treatment is limited to managing symptoms of hormonal hypersecretion and reducing tumor burden through systemic chemotherapy, to which the tumor invariably develops resistance (van der Zwan et al., 2013; Yao et al., 2008). Since the 1990s, the combination of streptozotocin, doxorubicin, and 5-fluorouracil has been the “gold standard” for advanced PanNETs (Moertel et al., 1980; Moertel et al., 1992). However, the 5-year survival for these patients is as low as 25% and a mere 4% for those with poorly differentiated tumors (Yao et al., 2008), and overall survival has not improved in >40 years (Halfdanarson et al., 2008a; Zhang et al., 2013). Treatment with targeted therapies, such as everolimus (an mTOR inhibitor) and sunitinib (a multi-kinase inhibitor), has prolonged progression-free survival of patients with metastatic PanNETs (Raymond et al., 2011; Yao et al., 2011), and both were FDA approved for this

indication in 2011. However, the benefits of these targeted agents are relatively modest (~6 month increase in progression-free survival). Most recently, peptide receptor radiotherapy (PRRT), which uses radiolabeled somatostatin receptor (SSTR) ligands, has shown highly promising outcomes in clinical trials for some patients with metastatic SSTR-expressing PanNETs, but the fraction of patients who respond and the long term outcomes remain unknown (Cives and Strosberg, 2017). As such, there continues to be urgent need for greater insight into the molecular biology of PanNETs and the development of better therapies.

Genetic loss-of-function studies in mice demonstrate that pancreatic neuroendocrine cells are critically dependent on the UPR for proper development and maintenance and gave us the idea of manipulating the UPR in pancreatic islet tumors. For example, homozygous genetic deletion of *Ire1*α *or Xbp1* during development or in adult β-cells results in β-cell dysfunction, defective insulin secretion and in the case of *Xbp1* deletion, β-cell death (Hassler et al., 2015; Lee et al., 2011; Tirasophon et al., 1998).

While healthy endocrine cells secrete large amounts of protein in response to appropriate signals, the vast majority of both functioning and nonfunctioning PanNETs constitutively hypersecretes one or more hormones (Metz and Jensen, 2008; Oberg and Eriksson, 2005), further burdening the ER. For example, while each normal pancreatic β-cell is capable of releasing an estimated 1 million molecules of insulin per minute (63), some “insulinoma” PanNET cells secrete over 10-fold higher amounts of this hormone even under hypoglycemic conditions (Scheuner and Kaufman, 2008). Clinically, these

PanNETs are categorized as “functioning” because they secrete hormones that cause visible symptoms. It is important to note, however that even clinically silent “nonfunctioning” PanNETs usually secrete high levels of multiple hormones and peptides (e.g., CgA, synaptophysin) that do not cause clinical symptoms, allowing these tumors to remain undetected until late stage. For example, elevated plasma levels of CgA are present in 60-100% of patients with nonfunctioning PanNETs and can be used to follow disease progression, response to therapy, and relapse (Baudin et al., 1998; Nobels et al., 1998; Pirker et al., 1998). Thus, although these PanNETs are characterized as “nonfunctioning” and are clinically undetectable, they still have abnormally high secretory demands. We therefore predicted that PanNETs, which have uncontrolled protein secretion and are subject to other ER stress insults *in vivo* (e.g., hypoxia), are even more dependent on the UPR than their healthy endocrine cell counterparts.

Indeed, we present evidence here of UPR hyperactivation, including the IRE1α/XBP1s axis, in human PanNET samples and INS-1 xenografts. The signaling outputs of the UPR in these tumors cells seem to be carefully balanced and biased towards adaptation. Moreover, INS-1 xenografts experience higher levels of ER stress and UPR activity compared with the same cells grown in culture, the implications of which became clear when we began to study the effects of forcibly activating or inhibiting the pathway on tumor growth *in vivo*.

Further hyperactivating IRE1α in INS-1 xenografts using Dox-induced expression switched the UPR outputs from survival to death, triggering tumor cell apoptosis and decreasing tumor burden. Type I kinase inhibitors of IRE1α can potentially mimic these effects by stabilizing its *active* kinase conformation, which allosterically activates IRE1α's RNase to trigger its apoptotic program (Ghosh et al., 2014; Mendez et al., 2015). Unfortunately, these inhibitors are not yet selective enough to use *in vivo.*

However, because PanNETs experience higher-than-normal levels of ER stress and UPR activation, we predicted that PanNETs would also be sensitive to the loss of these pro-homeostatic signals downstream of IRE1α. To test this hypothesis, we first used the CRISPR/Cas9 system to genetically inactivate *Ire1α* or *Xbp1*. The resulting decrease in tumor burden compared with INS-1 FRT/TO control tumors was dramatic. Importantly, while we observe no significant difference in rates of cell proliferation *in vitro,* INS-1 IRE1α KO and INS-1 XBP1 KO tumors *in vivo* are much less proliferative (Ki67 staining) than the parental lines or CRISPR/Cas-9 non-targeting controls. This reinforces the importance of our early observation that the INS-1 FRT tumors experience elevated ER stress and UPR activation *in vivo* versus *in vitro*, and that cells are critically reliant on the IRE1α/XBP1 arm only when they encounter stressful micro-environmental conditions. In culture, given all necessary nutrients, INS-1 cells do not need to activate IRE1α or downstream XBP1s, so deletion of these UPR components does not hinder their survival. In a tumor, however, these same INS-1 cells may experience greater hypoxia (particularly in the center of the tumor mass), ER stress, glucose deprivation, and other environmental stresses commonly found in solid tumors. Faced with these

stresses, they need a robust and active UPR, and the absence of IRE1α and adaptive XBP1s becomes a hindrance to their ability to thrive. We also find that *Ire1α* levels are elevated in INS-1 XBP1 KO tumors, reflecting efforts to respond to heightened ER stress and echoing previous findings that IRE1α activity increased in normal pancreatic β-cells in response to *Xbp1* deletion.

The promise of these results prompted us to study the effects of chemical inhibition of IRE1α. Our team recently developed first-in-class Type II ATP-competitive IRE1α *K*inase *I*nhibiting *R*Nase *A*ttenuators—*KIRAs*—that bind and stabilize IRE1α's kinase domain in the *inactivate* confirmation and allosterically inhibit its RNase. A more potent and highly selective KIRA, KIRA8, was then developed by Amgen, where the compound was tested on over 200 cancer cell lines, none of which were from PanNETs, for 48h. In that study, KIRA8 was found to have no effect on the viability of any of these cell lines in culture. However, as we have shown repeatedly, tumors confront hostile microenvironmental conditions *in vivo* that are not adequately mimicked *in vitro*. We tested KIRA8 on cultured INS-1 cells at concentrations that essentially shut off IRE1α activity (as measured by *Xbp1* splicing) and also found negligible effects on growth and survival for up to 6 days, consistent with our observations of the INS-1 IRE1α and INS-1 XBP1 KO cells. However, a completely different story emerges *in vivo*. Within 24h, tumors from KIRA8-treated animals have reduced *Xbp1* splicing (confirming on-target activity), decreased proliferation as measured by Ki67, and cell cycle arrest as indicated by p21 upregulation. This is consistent with reports in pre-B acute lymphoblastic leukemia and other cancers that IRE1α inhibition and loss of *Xbp1s* leads to cell cycle

arrest and cell death associated with increased p21 expression (Kharabi Masouleh et al., 2014; Sun et al., 2016). Moreover, after 24-48hr of KIRA8 treatment, the INS-1 tumors show upregulation of ER stress markers (Bip/GRP78), the apoptotic protein BIM, and begin undergoing apoptosis (Cleaved Casp3). This is consistent with findings in hematopoietic cells that *Xbp1s* has a direct anti-apoptotic effect, leading to decreases in pro-apoptotic *Bim* mRNA (Kurata et al., 2011). Hence, pharmacologic inhibition of IRE1α *in vivo* leaves tumor cells without a strong adaptive response and leads to rapid growth arrest and apoptosis of INS-1 tumors.

Notably, the KIRA8-treated INS-1 tumors show upregulation of markers of hypoxic and ischemic stress, suggesting that the absence of adaptive IRE1α signaling to counteract these stresses render tumor cells even more vulnerable to a destructive ER stress-induced apoptotic cascade. We can mimic these conditions *in vitro* by using Tunicamycin (Tm) to induce ER stress and apoptosis in a dose-dependent manner. Apoptosis is intensified by the addition of KIRA8 to Tm-treated cells. Together, our results lead to a working mechanistic model in which tumor cell fate is critically dependent on the balance of Adaptive vs. Terminal IRE1α outputs to handle ER stress conditions, and KIRA8 treatment disrupts this balance by removing the primary adaptive output, XBP1s (Figure 8). Under normal conditions, INS-1 tumors experience ER stress and activate IRE1α, which in turn increases the production of Adaptive XBP1s. XBP1s is responsible for transcriptional activation of many genes encoding proteins that help restore ER homeostasis as well as repression of senescence and apoptosis-inducing *p21* and *Bim*. The introduction of KIRA8 under these conditions of ER stress blocks

IRE1α dimerization and phosphorylation, thus preventing activation of XBP1s. The failure to turn on Adaptive signaling further increases ER stress, as indicated by the increase in *Bip* and *Ire1α* mRNA, which triggers BIM-mediated mitochondrial apoptosis. Because IRE1α and therefore XBP1s are inhibited, the counterbalance against *Bim* and p21 upregulation is missing. It remains to be clarified what mediates the ER stress-induced increase in BIM. We have not observed consistent compensatory increases in other arms of the UPR but cannot completely rule them out. Little is known about ATF6, and there are comparatively few tools that can be used to study it. It is also possible that this apoptotic pathway is mediated by IRE1α itself. In addition to its key role as an RNase, IRE1α has also been shown to be a scaffold for proteins such as ABL and JNK, the latter of which has also been shown to be upstream of BIM (Morita et al., 2017; Urano et al., 2000). It is important to note that although KIRA8 potently inhibits the IRE1α kinase (and allosterically the RNase), thus shutting down its enzymatic activities, IRE1α is still present in the cell and able to serve as a scaffold, though relatively little is known about that role (Morita et al., 2017).

When recipient mice are treated with KIRA8 for 3 weeks, their INS-1 tumors are about half the size of those of vehicle-treated animals. In sharp contrast to its lack of effect on INS-1 growth *in vitro*, KIRA8 administration results in significantly smaller tumors *in vivo*, a finding that phenocopies the INS-1 IRE1α KO cells grown *in vivo*. Not surprisingly, as KIRA8 administration resulted in only about a 50% decrease in IRE1α activity, as measured by XBP1, the effects on tumor growth are not as pronounced as those of genetically deleting *Ire1α*, which completely eliminates XBP1 splicing. With more potent

KIRAs, it should be possible to achieve greater anti-tumor effects. Notably, when we allow INS-1 tumors to grow for 2 weeks in the animals before beginning KIRA8 treatment, an experimental scheme that better mimics treatment of patients in the clinic, those tumors are also significantly smaller than tumors from vehicle-treated control animals. Importantly, no toxicity (including against normal islets) has been observed in tumor-bearing or healthy control mice for up to 2 months at the doses used. Moreover, as opposed to PERK inhibitors, which cause pancreatic β-cell toxicity within approximately 2 weeks of administration, first generation KIRA6 and second generation KIRA8 have been shown to have significant β-cell sparing effects in multiple diabetes models (Ghosh et al., 2014; Morita et al., 2017). However, it is worth noting that advanced PanNET is one clinical scenario where diabetes could be considered an acceptable toxicity in some patients (as is the case for the FDA-approved drug Streptozotocin).

To determine whether these results generalize to other PanNET models, we next tested KIRA8 in the well-characterized transgenic RIP-Tag2 model, which has been used as a preclinical PanNET model for over 20 years and has predicted the clinical efficacy of several compounds that have gone on to FDA-approval for pancreatic neuroendocrine tumors, including everolimus and sunitinib. In this model, the decreases in tumor burden were even more dramatic than in the INS-1 xenograft model. The pancreata of KIRA8-treated mice much more closely resembled those of wild-type control mice with no pancreatic tumors, and their tumors were generally invisible to the naked eye. In contrast, the pancreata of vehicle-treated mice were filled with grossly visible tumors.

Histologically, this translated to a striking decrease in tumor in the KIRA8 treated RIP-Tag2 mice. Most excitingly, when initiated at 12-weeks of age, KIRA8 treatment more than double the mean time of survival compared to the vehicle treated controls. Not only were the animals able to survive for a much longer period, but they also moved normally, gained weight, and appeared to be otherwise healthy. The biggest caveat of our treatment strategy was that the relative short half-life of KIRA8 in plasma required us to administer the drug by daily i.p. injections, which led to some inflammation around the injection site. The development of orally bioavailable IRE1α inhibitors would avoid the need for such injections.

Intriguingly, KIRA8 had a more dramatic effect in the RIP-Tag2 model compared with the INS-1 xenograft model. There are many differences between the two models that might explain the discrepancy, and those differences hint at possible combination therapies. One obvious difference between the two models is the lack of immune system in NSG mice. The recent explosion in immunotherapy suggests that the immune system has a more complex and widespread role in cancer than initially appreciated and may enhance the effects of KIRA8 in the RIP-Tag2 model. An impaired UPR may enhance the normal anti-tumor immune response by exposing tumor self-antigens.

Together, our data strongly argue that PanNET cells are much more sensitive to modest reductions in UPR outputs compared with healthy β-cells. Our data indicate that IRE1α and the UPR in general should be further explored as potential therapeutic targets in PanNETs and other hypersecretory cancers. Additional preclinical studies of

their effectiveness in combination with existing therapies for PanNETs and other cancers are needed. Moreover, because IRE1α inhibition is not dependent on the presence of a specific IRE1α mutation in any specific cancer, this strategy can be used on a larger population.

It is worth noting that advanced PanNET is one clinical scenario where diabetes could be considered an acceptable toxicity in some patients (as is the case for the FDA-approved drug Streptozotocin), but this makes IRE1α an even more appealing target than PERK despite the fact that both appear to have similar antitumor effects in the INS-1 model and was the reason we pursued the former route in greater depth. Further investigation is needed to determine the mechanism of PERK inhibition-induced decreases in tumor burden.

Materials and Methods

Human Samples

We obtained 6 deidentified primary human PanNETs and matched normal pancreata from the UCSF Department of Pathology, CHR protocol #. We also obtained 4 frozen human PanNET samples for RNA analysis.

Tissue Culture and Small Molecules

Generation of isogenic, stable INS-1 lines was described previously [9]. Brefeldin A (BFA) and Doxycycline were purchased from Sigma-Aldrich. KIRA8 was synthesized in house and purified by reverse phase chromatography (HPLC). The purity of KIRA6 was determined with two analytical RP-HPLC methods, using a Varian Microsorb-MV 100-5 C18 column (4.6 mm x 150 mm), and eluted with either H2O/CH3CN or H2O/ MeOH gradient solvent systems (+0.05% TFA) run over 30 min. Products were detected by UV at 254 nm. KIRA8 was found to be >95% pure in both solvent systems. For use in tissue culture, KIRA8 was dissolved in DMSO at a concentration of 20 mM. For use in animal studies, KIRA8 was dissolved in a vehicle solution (3% ethanol, 7% Tween-80, 1.2% ddH_2O, 88.8% 0.85% W/V saline) at a working concentration of 10 mg/ml.

CRISPR/Cas9

Guide RNAs were designed using the Zhang Lab's Optimized Design Tool (crispr.mit.edu) and targeted to the 5' end of each gene to create random insertions/deletions (indels) upstream of key structural and functional domains. For

each gRNA, forward and reverse oligonucleotides were purchased from Integrated DNA Technologies (listed in Table S1), annealed, and ligated into the pSpCas9(BB)-2A-EGFP vector (pX458; a gift from Feng Zhang; Addgene Plasmid #48138) at the BbsI cloning site. The resulting plasmids were transfected into INS-1 cells using Lipofectamine 2000 (Thermo Fisher Scientific); a BD FACSAria II (BD Biosciences) was used to subsequently single-cell sort EGFP-positive cells and establish clonal lines. Clones were screened for knockout of target genes by Western Blot or by sequencing with custom primers (Integrated DNA Technologies; listed in Table S2), KAPA Mouse Genotyping Kit (KAPA Biosystems), and TOPO TA Cloning Kit (Life Technologies).

Western Blot and Antibodies

For protein analysis, cells were lysed in M-PER buffer (Thermo Fisher Scientific) plus phosphatase inhibitor cocktail (Cell Signaling Technologies). Protein concentration was determined using BCA Protein Assay (Thermo Fisher Scientific). Western blots were performed using 10% and 4-10% gradient Bis-Tris precast gels (NuPage) on Invitrogen XCell SureLock Mini-Cell modules. Gels were run using MES buffer and transferred onto nitrocellulose transfer membrane using an XCell II Blot Module or iBlot 2 Dry Blotting System (Thermo Fisher Scientific). Antibody binding was visualized on CL-XPosure film using ECL SuperSignal West Dura Extended Duration Substrate (both from Thermo Fisher Scientific) or using the Odyssey CLx Imaging System (LI-COR Biosciences). Antibodies used: IRE1α (Cell Signaling Technology #3294), IRE1α p-S724 (Novus Biologicals #NB100-2323), PERK (CST #3192), PERK p-T980 (CST #3179), eIF2α (CST #9722), eIF2α p-S51 (CST #3398); Spliced XBP-1 (BioLegend

#619502), p21 (BD 556431, 1:500), actin (Sigma A5441 1:3000), Bax (CST #2772), Bak (CST #3814), CHOP (CST #2895), ATF4 (CST #11815), Insulin (CST #8138), BIM (CST #2933), GLUT1 (abcam 115730), GLUT2 (ab95256)

RNA Isolation, Quantitative Real-Time PCR, and Primers

RNA was isolated from whole cells using either Qiashredder and RNeasy kits (Qiagen) or Trizol (Invitrogen). TissueLyser II (Qiagen) was used for RNA isolation from tumors. For cDNA synthesis, 500-1000 ng total RNA was reverse transcribed using Superscript II Reverse Transcriptase and Oligo $d(T)_{16}$ primer (Invitrogen). For qPCR, we used Power SYBR Green and the StepOnePlus Real-Time PCR System (Applied Biosystems). qPCR primers are listed in Table S3. Gene expression levels were normalized to GAPDH or Actin, as indicated.

XBP-1 mRNA splicing

RNA was isolated from whole cells or tissue and reverse transcribed as detailed above to obtain total cDNA. Sense (5'-AGGAAACTGAAAAACAGAGTAGCAGC-3') and antisense (5'-TCCTTCTGGGTAGACCTCTGG-3') primers were used in a standard PCR reaction to amplify a region spanning the 26-nucleotide intron that includes a single PstI restriction site and is excised by active IRE1α. The resulting PCR fragments were then digested by PstI (New England Biolabs), resolved on 3% agarose gels, stained with ethidium bromide and quantified by densitometry using ImageJ (U. S. National Institutes of Health).

Cell Growth and Apoptosis Assays

To measure apoptosis by Annexin V staining, cells were plated in 12-well plates overnight. Cells were then treated as described for indicated times. On the day of analysis, cells were trypsinized, washed in PBS, and resuspended in Annexin V binding buffer (10 mM HEPES 7.4, 140 mM NaCl, 2.5 mM $CaCl_2$) with Annexin-V FITC (BD Biosciences). Flow cytometry was performed on a Becton Dickinson LSRFortessa or LSRII flow cytometer. To measure cell proliferation, cells were seeded at 5-10% confluence in 96-well plates, treated as indicated, and assayed using the CellTiter-Glo Luminescent Cell Viability Assay (Promega) according to the manufacturer's protocol. Luminescence was quantified using a Cytation 5 Cell Imaging Multi-Mode Reader (BioTek).

Animal Studies

Xenografts

5-8 week old NOD.Cg-*Prkdc*^{scid} *Il2rg*^{tm1Wjl}/SzJ (NSG, Stock #005557, The Jackson Laboratory) mice were injected s.c. with 5 x 10^6 INS-1 cells, and tumor size was followed for up to 4 weeks. Where indicated, KIRA8 or vehicle solutions were prepared as described above and delivered daily by intraperitoneal injection,

RIP-Tag2

Tg(RIP1-Tag)2Dh mice (previously described in Hanahan, 1985) were initially obtained from the Bergers Lab at UCSF and maintained as heterozygotes by breeding wild-type C57BL/6 female mice with hemizygous RIP-Tag2 male mice. RIP-Tag2-positive mice were given supplemental diet with adjusted sucrose (Teklad Custom Research Diets).

KIRA8 treatment, as described above, was initiated at 12 weeks and continued as described. All animal studies were reviewed and approved by the UCSF Institutional Animal Care and Use Committee. Animals were maintained in a specific pathogen-free animal facility on a 12hr light–dark cycle at an ambient temperature of 21°C. They were given free access to water and food.

Blood Collection

To monitor blood glucose levels, a drop of blood was collected from the tail onto OneTouch® Ultra® Blue test strips and measured using the OneTouch® Ultra® 2 Meter (LifeScan).

Histology and Immunostaining

Samples were fixed in 4% buffered formaldehyde for 24h, washed in PBS, transferred into 70% EtOH in ddH_2O, and then embedded in paraffin and sectioned (5mm thickness) using a Leica RM2255 rotary microtome or by the Brain Tumor Research Center (BTRC) Histology Core at UCSF. Hematoxylin and eosin staining was performed using standard methods. Stained slides were imaged using a Leica DM LB microscope and NIS-Elements F software (version 3.2); [add 11th floor confocal scope and software info]; or a Zeiss AxioOberver Z1 inverted microscope and ZEN pro 2012 software. Antibodies used for immunohistochemistry: chromogranin A [polyclonal] (Cell Marque, 1:4), synaptophysin [LK2H10 clone] (Cell Marque, 1:100), insulin (DAKO A0564, 1:200), cleaved caspase 3 (CST #9664 1:2000), BiP [C50B12] (CST #3177, 1:200), CD31 (CST #77699 1:100), Myc (Sigma M4439, 1:5000), IRE1α (CST #3294, 1:100), Bim [C34C5] (CST #2933), GLUT1 [EPR3915] (ab115730, 1:500).

For TUNEL, samples were stained using the ApopTag Red In Situ Apoptosis Detection Kit (Millipore) according to the manufacturer's instructions. Samples were also costained with DAPI (Sigma) before mounting onto slides with VectaShield (Vector Laboratories).

Image Analysis and Statistics

Images were analyzed using Image J software (NIH). Ki67 images were quantified using the IHC Profiler plugin for Image J. All other images were quantified manually in a blinded fashion. Statistical analyses are expressed as means +/- standard deviation. Significance was determined by two-tailed Student's *t*-test and graphed using Prism 6 software. Graphs represent the average of at least 3 independent experiments. *P* value < 0.05 was considered statistically significant.

References

Aragon, T., van Anken, E., Pincus, D., Serafimova, I.M., Korennykh, A.V., Rubio, C.A., and Walter, P. (2008). Messenger RNA targeting to endoplasmic reticulum stress signalling sites. Nature.

Aragon, T., van Anken, E., Pincus, D., Serafimova, I.M., Korennykh, A.V., Rubio, C.A., and Walter, P. (2009). Messenger RNA targeting to endoplasmic reticulum stress signalling sites. Nature *457*, 736-740.

Asfari, M., Janjic, D., Meda, P., Li, G., Halban, P.A., and Wollheim, C.B. (1992). Establishment of 2-mercaptoethanol-dependent differentiated insulin-secreting cell lines. Endocrinology *130*, 167-178.

Auf, G., Jabouille, A., Guerit, S., Pineau, R., Delugin, M., Bouchecareilh, M., Magnin, N., Favereaux, A., Maitre, M., Gaiser, T.*, et al.* (2010). Inositol-requiring enzyme 1alpha is a key regulator of angiogenesis and invasion in malignant glioma. Proc Natl Acad Sci U S A *107*, 15553-15558.

Babu, V., Paul, N., and Yu, R. (2013). Animal models and cell lines of pancreatic neuroendocrine tumors. Pancreas *42*, 912-923.

Baudin, E., Gigliotti, A., Ducreux, M., Ropers, J., Comoy, E., Sabourin, J.C., Bidart, J.M., Cailleux, A.F., Bonacci, R., Ruffie, P.*, et al.* (1998). Neuron-specific enolase and chromogranin A as markers of neuroendocrine tumours. Br J Cancer *78*, 1102-1107.

Bergers, G., Javaherian, K., Lo, K.M., Folkman, J., and Hanahan, D. (1999). Effects of angiogenesis inhibitors on multistage carcinogenesis in mice. Science *284*, 808-812.

Bobrovnikova-Marjon, E., Grigoriadou, C., Pytel, D., Zhang, F., Ye, J., Koumenis, C., Cavener, D., and Diehl, J.A. (2010). PERK promotes cancer cell proliferation and tumor growth by limiting oxidative DNA damage. Oncogene *29*, 3881-3895.

Carrasco, D.R., Sukhdeo, K., Protopopova, M., Sinha, R., Enos, M., Carrasco, D.E., Zheng, M., Mani, M., Henderson, J., Pinkus, G.S.*, et al.* (2007). The differentiation and stress response factor XBP-1 drives multiple myeloma pathogenesis. Cancer Cell *11*, 349-360.

Chen, X., Ding, Y., Liu, C.G., Mikhail, S., and Yang, C.S. (2002). Overexpression of glucose-regulated protein 94 (Grp94) in esophageal adenocarcinomas of a rat surgical model and humans. Carcinogenesis *23*, 123-130.

Chen, X., Iliopoulos, D., Zhang, Q., Tang, Q., Greenblatt, M.B., Hatziapostolou, M., Lim, E., Tam, W.L., Ni, M., Chen, Y.*, et al.* (2014). XBP1 promotes triple-negative breast cancer by controlling the HIF1alpha pathway. Nature *508*, 103-107.

Cives, M., and Strosberg, J. (2017). Radionuclide Therapy for Neuroendocrine Tumors. Curr Oncol Rep *19*, 9.

Credle, J.J., Finer-Moore, J.S., Papa, F.R., Stroud, R.M., and Walter, P. (2005). Inaugural Article: On the mechanism of sensing unfolded protein in the endoplasmic reticulum. Proc Natl Acad Sci U S A *102*, 18773-18784.

Dejeans, N., Manie, S., Hetz, C., Bard, F., Hupp, T., Agostinis, P., Samali, A., and Chevet, E. (2014). Addicted to secrete - novel concepts and targets in cancer therapy. Trends Mol Med *20*, 242-250.

Delepine, M., Nicolino, M., Barrett, T., Golamaully, M., Lathrop, G.M., and Julier, C. (2000). EIF2AK3, encoding translation initiation factor 2-alpha kinase 3, is mutated in patients with Wolcott-Rallison syndrome. Nat Genet *25*, 406-409.

Fernandez, P.M., Tabbara, S.O., Jacobs, L.K., Manning, F.C., Tsangaris, T.N., Schwartz, A.M., Kennedy, K.A., and Patierno, S.R. (2000). Overexpression of the glucose-regulated stress gene GRP78 in malignant but not benign human breast lesions. Breast Cancer Res Treat *59*, 15-26.

Gardner, B.M., and Walter, P. (2011). Unfolded proteins are Ire1-activating ligands that directly induce the unfolded protein response. Science *333*, 1891-1894.

Ghosh, R., Wang, L., Wang, E.S., Perera, B.G., Igbaria, A., Morita, S., Prado, K., Thamsen, M., Caswell, D., Macias, H.*, et al.* (2014). Allosteric Inhibition of the IRE1alpha RNase Preserves Cell Viability and Function during Endoplasmic Reticulum Stress. Cell *158*, 534-548.

Gortz, B., Roth, J., Krahenmann, A., de Krijger, R.R., Muletta-Feurer, S., Rutimann, K., Saremaslani, P., Speel, E.J., Heitz, P.U., and Komminoth, P. (1999). Mutations and allelic deletions of the MEN1 gene are associated with a subset of sporadic endocrine pancreatic and neuroendocrine tumors and not restricted to foregut neoplasms. Am J Pathol *154*, 429-436.

Greenman, C., Stephens, P., Smith, R., Dalgliesh, G.L., Hunter, C., Bignell, G., Davies, H., Teague, J., Butler, A., Stevens, C.*, et al.* (2007). Patterns of somatic mutation in human cancer genomes. Nature *446*, 153-158.

Halfdanarson, T.R., Rabe, K.G., Rubin, J., and Petersen, G.M. (2008a). Pancreatic neuroendocrine tumors (PNETs): incidence, prognosis and recent trend toward improved survival. Ann Oncol *19*, 1727-1733.

Halfdanarson, T.R., Rubin, J., Farnell, M.B., Grant, C.S., and Petersen, G.M. (2008b). Pancreatic endocrine neoplasms: epidemiology and prognosis of pancreatic endocrine tumors. Endocrine-related cancer *15*, 409-427.

Han, D., Lerner, A.G., Vande Walle, L., Upton, J.P., Xu, W., Hagen, A., Backes, B.J., Oakes, S.A., and Papa, F.R. (2009). IRE1alpha kinase activation modes control alternate endoribonuclease outputs to determine divergent cell fates. Cell *138*, 562-575.

Hanahan, D. (1985). Heritable formation of pancreatic beta-cell tumours in transgenic mice expressing recombinant insulin/simian virus 40 oncogenes. Nature *315*, 115-122.

Harrington, P.E., Biswas, K., Malwitz, D., Tasker, A.S., Mohr, C., Andrews, K.L., Dellamaggiore, K., Kendall, R., Beckmann, H., Jaeckel, P.*, et al.* (2015). Unfolded Protein Response in Cancer: IRE1alpha Inhibition by Selective Kinase Ligands Does Not Impair Tumor Cell Viability. ACS Med Chem Lett *6*, 68-72.

Hassler, J.R., Scheuner, D.L., Wang, S., Han, J., Kodali, V.K., Li, P., Nguyen, J., George, J.S., Davis, C., Wu, S.P.*, et al.* (2015). The IRE1alpha/XBP1s Pathway Is Essential for the Glucose Response and Protection of beta Cells. PLoS Biol *13*, e1002277.

Hetz, C., Chevet, E., and Oakes, S.A. (2015). Proteostasis control by the unfolded protein response. Nat Cell Biol *17*, 829-838.

Hollien, J., Lin, J.H., Li, H., Stevens, N., Walter, P., and Weissman, J.S. (2009). Regulated Ire1-dependent decay of messenger RNAs in mammalian cells. J Cell Biol *186*, 323-331.

Horne, S.D., Chowdhury, S.K., and Heng, H.H. (2014). Stress, genomic adaptation, and the evolutionary trade-off. Front Genet *5*, 92.

Jamora, C., Dennert, G., and Lee, A.S. (1996). Inhibition of tumor progression by suppression of stress protein GRP78/BiP induction in fibrosarcoma B/C10ME. Proc Natl Acad Sci U S A *93*, 7690-7694.

Kharabi Masouleh, B., Geng, H., Hurtz, C., Chan, L.N., Logan, A.C., Chang, M.S., Huang, C., Swaminathan, S., Sun, H., Paietta, E.*, et al.* (2014). Mechanistic rationale for targeting the unfolded protein response in pre-B acute lymphoblastic leukemia. Proc Natl Acad Sci U S A *111*, E2219-2228.

Kosmaczewski, S.G., Edwards, T.J., Han, S.M., Eckwahl, M.J., Meyer, B.I., Peach, S., Hesselberth, J.R., Wolin, S.L., and Hammarlund, M. (2014). The RtcB RNA ligase is an essential component of the metazoan unfolded protein response. EMBO Rep *15*, 1278-1285.

Koumenis, C. (2006). ER stress, hypoxia tolerance and tumor progression. Curr Mol Med *6*, 55-69.

Kurata, M., Yamazaki, Y., Kanno, Y., Ishibashi, S., Takahara, T., Kitagawa, M., and Nakamura, T. (2011). Anti-apoptotic function of Xbp1 as an IL-3 signaling molecule in hematopoietic cells. Cell Death Dis *2*, e118.

Lee, A.H., Heidtman, K., Hotamisligil, G.S., and Glimcher, L.H. (2011). Dual and opposing roles of the unfolded protein response regulated by IRE1alpha and XBP1 in proinsulin processing and insulin secretion. Proc Natl Acad Sci U S A *108*, 8885-8890.

Lee, A.H., Iwakoshi, N.N., and Glimcher, L.H. (2003). XBP-1 regulates a subset of endoplasmic reticulum resident chaperone genes in the unfolded protein response. Mol Cell Biol *23*, 7448-7459.

Lee, A.S., and Hendershot, L.M. (2006). ER stress and cancer. Cancer Biol Ther *5*, 721-722.
Lerner, A.G., Upton, J.P., Praveen, P.V., Ghosh, R., Nakagawa, Y., Igbaria, A., Shen, S., Nguyen, V., Backes, B.J., Heiman, M.*, et al.* (2012). IRE1alpha induces thioredoxin-interacting protein to activate the NLRP3 inflammasome and promote programmed cell death under irremediable ER stress. Cell Metab *16*, 250-264.

Lu, Y., Liang, F.X., and Wang, X. (2014). A synthetic biology approach identifies the mammalian UPR RNA ligase RtcB. Mol Cell *55*, 758-770.

Ma, Y., and Hendershot, L.M. (2004). The role of the unfolded protein response in tumour development: friend or foe? Nat Rev Cancer *4*, 966-977.

McCracken, A.A., and Brodsky, J.L. (2003). Evolving questions and paradigm shifts in endoplasmic-reticulum-associated degradation (ERAD). Bioessays *25*, 868-877.

Mendez, A.S., Alfaro, J., Morales-Soto, M.A., Dar, A.C., McCullagh, E., Gotthardt, K., Li, H., Acosta-Alvear, D., Sidrauski, C., Korennykh, A.V.*, et al.* (2015). Endoplasmic reticulum stress-independent activation of unfolded protein response kinases by a small molecule ATP-mimic. eLife *4*.

Metz, D.C., and Jensen, R.T. (2008). Gastrointestinal neuroendocrine tumors: pancreatic endocrine tumors. Gastroenterology *135*, 1469-1492.

Meusser, B., Hirsch, C., Jarosch, E., and Sommer, T. (2005). ERAD: the long road to destruction. Nat Cell Biol *7*, 766-772.

Moenner, M., Pluquet, O., Bouchecareilh, M., and Chevet, E. (2007). Integrated endoplasmic reticulum stress responses in cancer. Cancer Res *67*, 10631-10634.

Moertel, C.G., Hanley, J.A., and Johnson, L.A. (1980). Streptozocin alone compared with streptozocin plus fluorouracil in the treatment of advanced islet-cell carcinoma. N Engl J Med *303*, 1189-1194.

Moertel, C.G., Lefkopoulo, M., Lipsitz, S., Hahn, R.G., and Klaassen, D. (1992). Streptozocin-doxorubicin, streptozocin-fluorouracil or chlorozotocin in the treatment of advanced islet-cell carcinoma. N Engl J Med *326*, 519-523.

Morita, S., Villalta, S.A., Feldman, H.C., Register, A.C., Rosenthal, W., Hoffmann-Petersen, I.T., Mehdizadeh, M., Ghosh, R., Wang, L., Colon-Negron, K.*, et al.* (2017). Targeting ABL-IRE1alpha Signaling Spares ER-Stressed Pancreatic beta Cells to Reverse Autoimmune Diabetes. Cell Metab *25*, 883-897 e888.

Nobels, F.R., Kwekkeboom, D.J., Bouillon, R., and Lamberts, S.W. (1998). Chromogranin A: its clinical value as marker of neuroendocrine tumours. European journal of clinical investigation *28*, 431-440.

Oakes, S.A. (2017). Endoplasmic reticulum proteostasis: a key checkpoint in cancer. Am J Physiol Cell Physiol *312*, C93-C102.

Oakes, S.A., and Papa, F.R. (2015). The role of endoplasmic reticulum stress in human pathology. Annu Rev Pathol *10*, 173-194.

Oberg, K., and Eriksson, B. (2005). Endocrine tumours of the pancreas. Best practice & research Clinical gastroenterology *19*, 753-781.

Park, H.R., Tomida, A., Sato, S., Tsukumo, Y., Yun, J., Yamori, T., Hayakawa, Y., Tsuruo, T., and Shin-ya, K. (2004). Effect on tumor cells of blocking survival response to glucose deprivation. J Natl Cancer Inst *96*, 1300-1310.

Pirker, R.A., Pont, J., Pohnl, R., Schutz, W., Griesmacher, A., and Muller, M.M. (1998). Usefulness of chromogranin A as a marker for detection of relapses of carcinoid tumours. Clinical chemistry and laboratory medicine : CCLM / FESCC *36*, 837-840.

Raymond, E., Dahan, L., Raoul, J.L., Bang, Y.J., Borbath, I., Lombard-Bohas, C., Valle, J., Metrakos, P., Smith, D., Vinik, A.*, et al.* (2011). Sunitinib malate for the treatment of pancreatic neuroendocrine tumors. N Engl J Med *364*, 501-513.

Reid, M.D., Saka, B., Balci, S., Goldblum, A.S., and Adsay, N.V. (2014). Molecular genetics of pancreatic neoplasms and their morphologic correlates: an update on recent advances and potential diagnostic applications. American journal of clinical pathology *141*, 168-180.

Romero-Ramirez, L., Cao, H., Nelson, D., Hammond, E., Lee, A.H., Yoshida, H., Mori, K., Glimcher, L.H., Denko, N.C., Giaccia, A.J.*, et al.* (2004). XBP1 is essential for survival under hypoxic conditions and is required for tumor growth. Cancer Res *64*, 5943-5947.

Ruggero, D. (2013). Translational control in cancer etiology. Cold Spring Harb Perspect Biol *5*.

Salaria, S.N., and Shi, C. (2016). Pancreatic Neuroendocrine Tumors. Surg Pathol Clin *9*, 595-617.

Scarpa, A., Chang, D.K., Nones, K., Corbo, V., Patch, A.M., Bailey, P., Lawlor, R.T., Johns, A.L., Miller, D.K., Mafficini, A.*, et al.* (2017). Whole-genome landscape of pancreatic neuroendocrine tumours. Nature *543*, 65-71.

Scheuner, D., and Kaufman, R.J. (2008). The unfolded protein response: a pathway that links insulin demand with beta-cell failure and diabetes. Endocr Rev *29*, 317-333.

Schubert, U., Anton, L.C., Gibbs, J., Norbury, C.C., Yewdell, J.W., and Bennink, J.R. (2000). Rapid degradation of a large fraction of newly synthesized proteins by proteasomes. Nature *404*, 770-774.

Sevier, C.S., and Kaiser, C.A. (2002). Formation and transfer of disulphide bonds in living cells. Nat Rev Mol Cell Biol *3*, 836-847.

Shore, G.C., Papa, F.R., and Oakes, S.A. (2011). Signaling cell death from the endoplasmic reticulum stress response. Curr Opin Cell Biol *23*, 143-149.

Shuda, M., Kondoh, N., Imazeki, N., Tanaka, K., Okada, T., Mori, K., Hada, A., Arai, M., Wakatsuki, T., Matsubara, O.*, et al.* (2003). Activation of the ATF6, XBP1 and grp78 genes in human hepatocellular carcinoma: a possible involvement of the ER stress pathway in hepatocarcinogenesis. J Hepatol *38*, 605-614.

Smith, M.H., Ploegh, H.L., and Weissman, J.S. (2011). Road to ruin: targeting proteins for degradation in the endoplasmic reticulum. Science *334*, 1086-1090.

Song, M.S., Park, Y.K., Lee, J.H., and Park, K. (2001). Induction of glucose-regulated protein 78 by chronic hypoxia in human gastric tumor cells through a protein kinase C-epsilon/ERK/AP-1 signaling cascade. Cancer Res *61*, 8322-8330.

Sun, H., Lin, D.C., Guo, X., Kharabi Masouleh, B., Gery, S., Cao, Q., Alkan, S., Ikezoe, T., Akiba, C., Paquette, R.*, et al.* (2016). Inhibition of IRE1alpha-driven pro-survival pathways is a promising therapeutic application in acute myeloid leukemia. Oncotarget *7*, 18736-18749.

Tirasophon, W., Welihinda, A.A., and Kaufman, R.J. (1998). A stress response pathway from the endoplasmic reticulum to the nucleus requires a novel bifunctional protein kinase/endoribonuclease (Ire1p) in mammalian cells. Genes Dev *12*, 1812-1824.

Tollefsbol, T.O., and Cohen, H.J. (1990). The protein synthetic surge in response to mitogen triggers high glycolytic enzyme levels in human lymphocytes and occurs prior to DNA synthesis. Biochem Med Metab Biol *44*, 282-291.

Tu, B.P., and Weissman, J.S. (2004). Oxidative protein folding in eukaryotes: mechanisms and consequences. J Cell Biol *164*, 341-346.

Tuveson, D., and Hanahan, D. (2011). Translational medicine: Cancer lessons from mice to humans. Nature *471*, 316-317.

Upton, J.P., Wang, L., Han, D., Wang, E.S., Huskey, N.E., Lim, L., Truitt, M., McManus, M.T., Ruggero, D., Goga, A.*, et al.* (2012). IRE1alpha cleaves select microRNAs during ER stress to derepress translation of proapoptotic Caspase-2. Science *338*, 818-822.

Urano, F., Wang, X., Bertolotti, A., Zhang, Y., Chung, P., Harding, H.P., and Ron, D. (2000). Coupling of stress in the ER to activation of JNK protein kinases by transmembrane protein kinase IRE1. Science *287*, 664-666.

van der Zwan, J.M., Trama, A., Otter, R., Larranaga, N., Tavilla, A., Marcos-Gragera, R., Dei Tos, A.P., Baudin, E., Poston, G., Links, T.*, et al.* (2013). Rare neuroendocrine tumours: results of the surveillance of rare cancers in Europe project. European journal of cancer *49*, 2565-2578.

Xue, Z., He, Y., Ye, K., Gu, Z., Mao, Y., and Qi, L. (2011). A conserved structural determinant located at the interdomain region of mammalian inositol-requiring enzyme 1alpha. J Biol Chem *286*, 30859-30866.

Yao, J.C., Hassan, M., Phan, A., Dagohoy, C., Leary, C., Mares, J.E., Abdalla, E.K., Fleming, J.B., Vauthey, J.N., Rashid, A.*, et al.* (2008). One hundred years after "carcinoid": epidemiology of and prognostic factors for neuroendocrine tumors in 35,825 cases in the United States. J Clin Oncol *26*, 3063-3072.

Yao, J.C., Shah, M.H., Ito, T., Bohas, C.L., Wolin, E.M., Van Cutsem, E., Hobday, T.J., Okusaka, T., Capdevila, J., de Vries, E.G.*, et al.* (2011). Everolimus for advanced pancreatic neuroendocrine tumors. N Engl J Med *364*, 514-523.

Zhang, J., Francois, R., Iyer, R., Seshadri, M., Zajac-Kaye, M., and Hochwald, S.N. (2013). Current understanding of the molecular biology of pancreatic neuroendocrine tumors. J Natl Cancer Inst *105*, 1005-1017.

Zhou, J., Liu, C.Y., Back, S.H., Clark, R.L., Peisach, D., Xu, Z., and Kaufman, R.J. (2006). The crystal structure of human IRE1 luminal domain reveals a conserved dimerization interface required for activation of the unfolded protein response. Proc Natl Acad Sci U S A *103*, 14343-14348.

Appendix

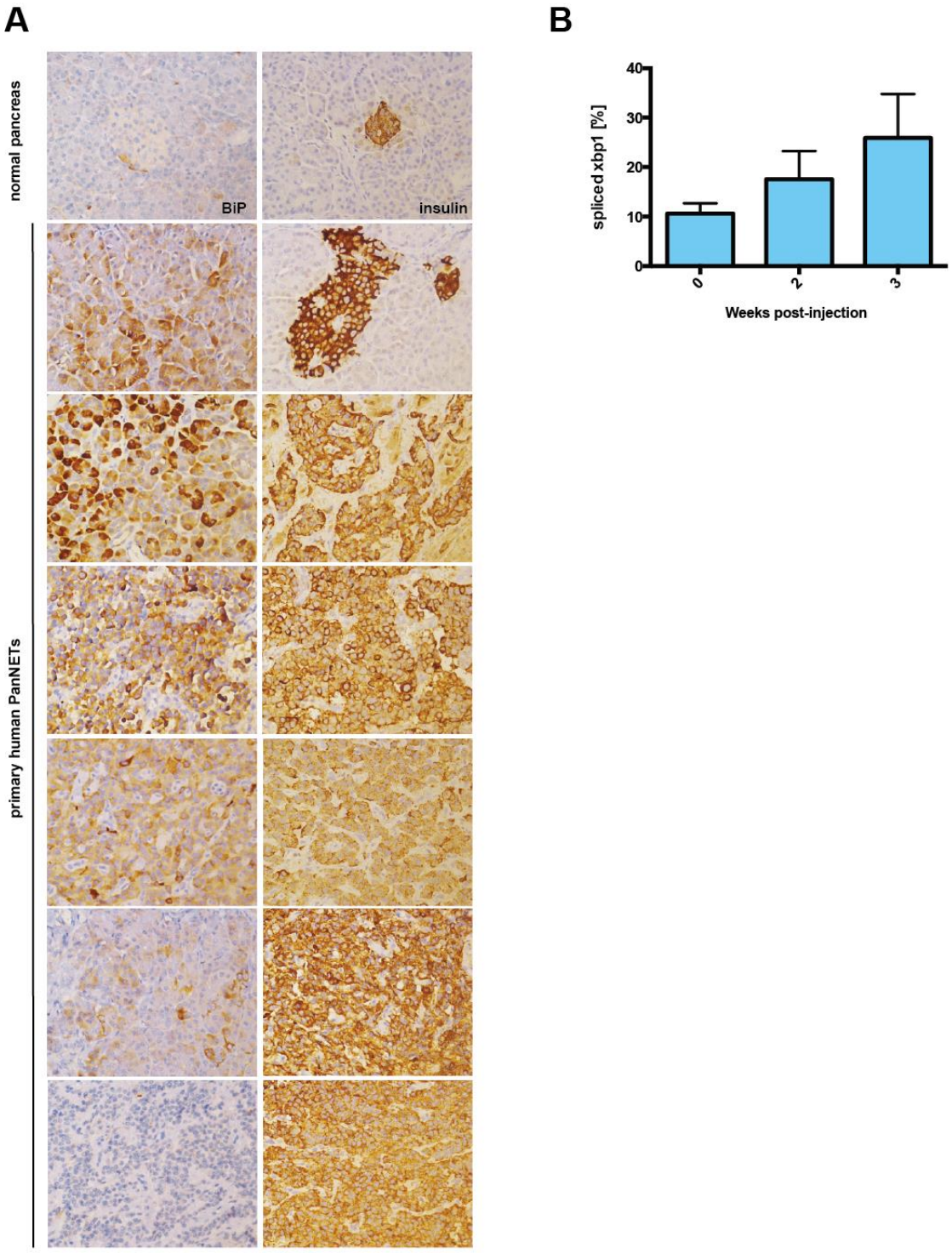

Supplemental Figure 1. Majority of primary human PanNETs show high ER stress. A. IHC for BiP/GRP78 (left) and insulin (right) on normal human pancreas (top row) and a panel of 6 primary human PanNETs. B. Spliced Xbp1 in INS1 FRT/TO tumors removed at specified weeks post-cell-injection.

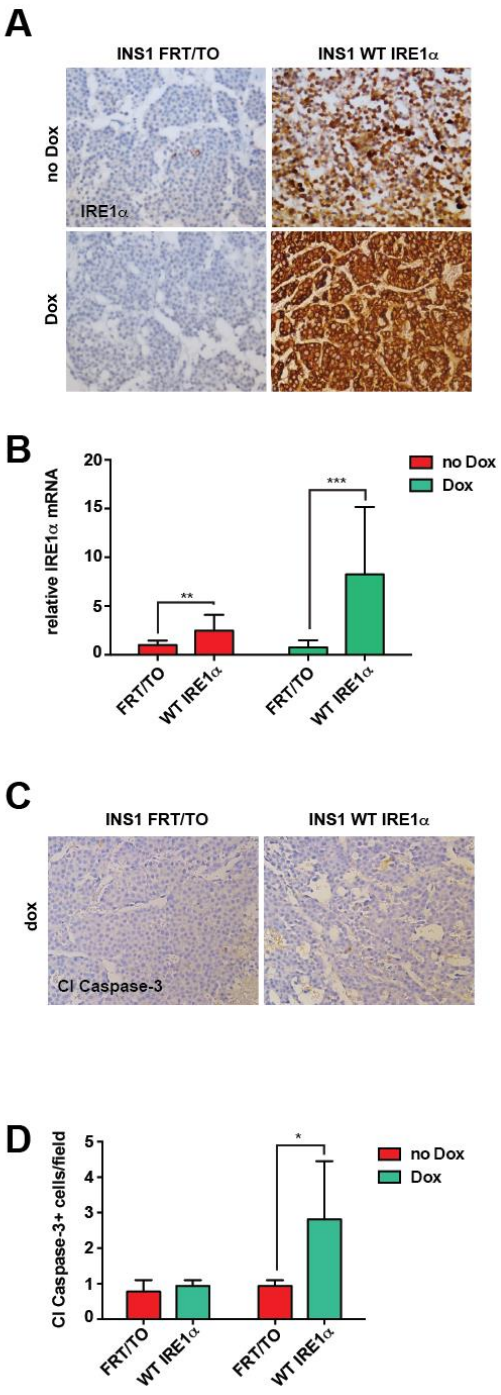

Supplemental Figure 2. Hyperactivation of WT IRE1α leads to apoptosis.
A. Representative images of IRE1α staining in INS-1 xenograft tumors at 4 weeks post-injection. B. Quantification of *Ire1α* mRNA in INS-1 xenograft tumors at 4 weeks post-injection. C. Representative images of Cleaved Caspase-3 in INS-1 xenograft tumors at 4 weeks post-injection. D. Quantification of Cleaved Caspase-3-positive cells in INS-1 xenograft tumors at 4 weeks post-injection. At least 4 samples were stained for each group, and at least 5 high powered fields (40x magnification) were imaged and manually counted for each sample. p=0.013.

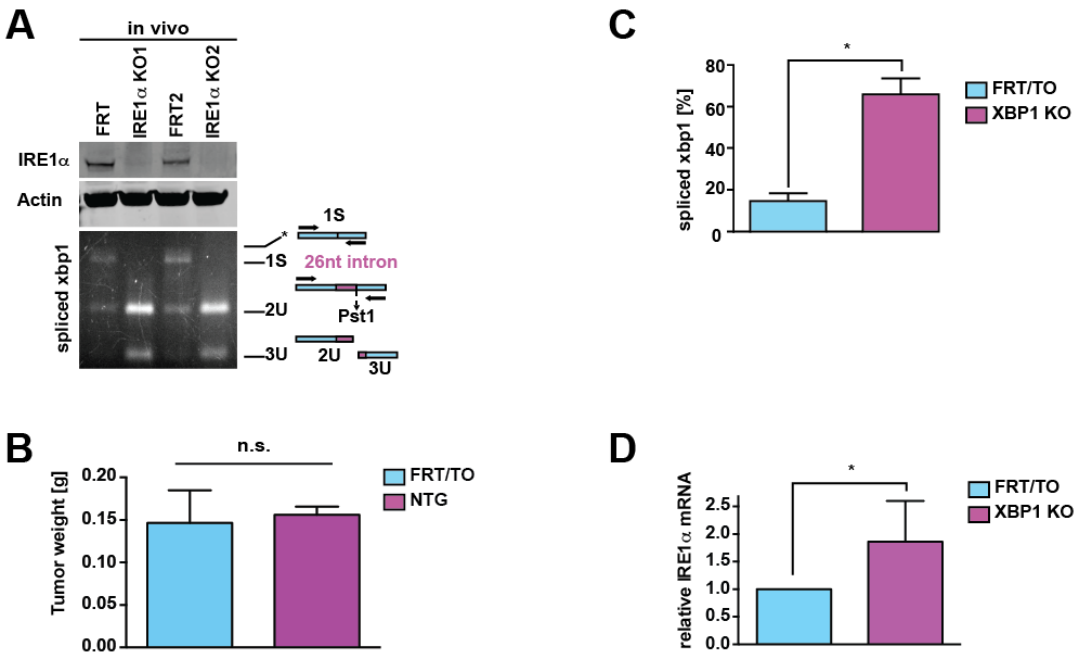

Supplemental Figure 3. CRISPR/Cas9 mediated deletion of *Ire1α* or *Xbp1* in INS-1 FRT/TO cells has dramatic effects, in contrast to a non-targeting CRISPR/Cas9 control

A. Top: Immunoblot showing IRE1α expression in INS-1 IRE1α KO cells compared with INS-1 FRT/TO cells *in vivo*. Actin was used as a loading control. Bottom: Gel showing *xbp1* splicing (second band from the top) with a diagram of the assay to the right. B. Weights of INS-1 FRT/TO xenograft tumors that were unaltered or had a nontargeting (NTG) CRISPR/Cas9 guide. n=3 per group, n.s.=not significant. C. Percent spliced *xbp1* in INS-1 FRT/TO vs INS-1 XBP1 KO tumors at 4 weeks post-injection. n=4 per group, p=0.029. D. Relative *Ire1α* mRNA in INS-1 FRT/TO vs INS-1 XBP1 KO tumors at 4 weeks post-injection. n=5 per group, p=0.032.

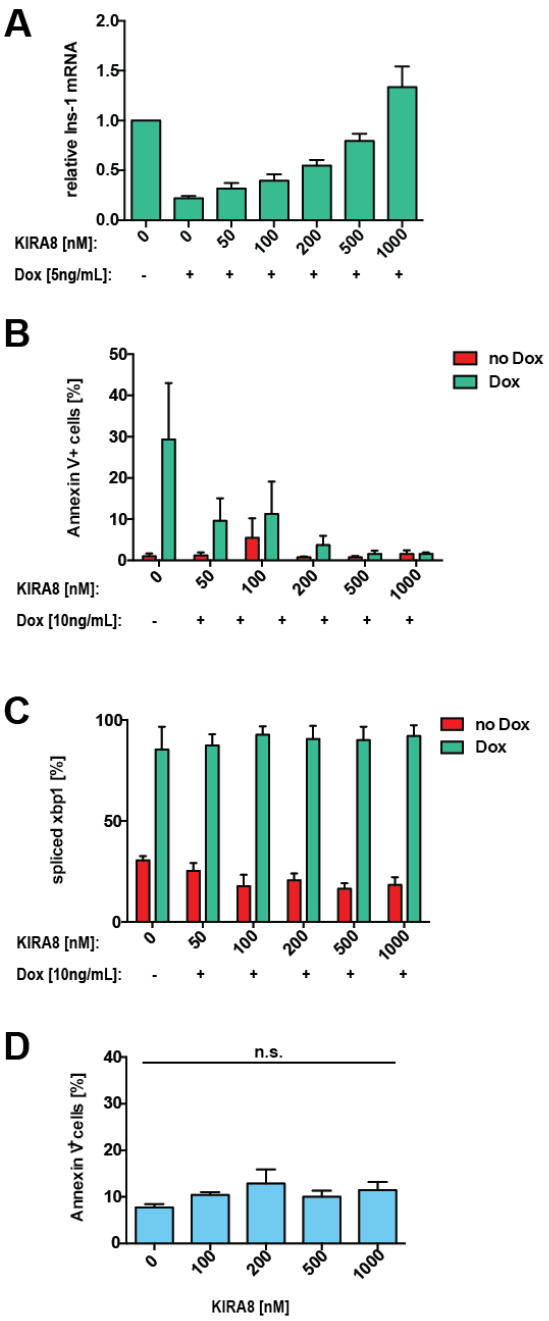

Supplemental Figure 4. Characterization of KIRA8 *in vitro*.
A. Relative *Ins-1* mRNA in INS-1 WT IRE1α cells treated with specified concentrations of KIRA8 and doxycycline for 3 days.
B. Percent Annexin V-positive INS-1 WT IRE1α cells treated with specified concentrations of KIRA8 and doxycycline for 3 days.
C. Percent spliced *xbp1* in INS-1 WT IRE1α cells treated with specified concentrations of KIRA8 and doxycycline for 3 days.
D. Percent Annexin V-positive INS-1 FRT/TO cells treated with specified concentrations of KIRA8 for 5 days. n.s.=not significant.

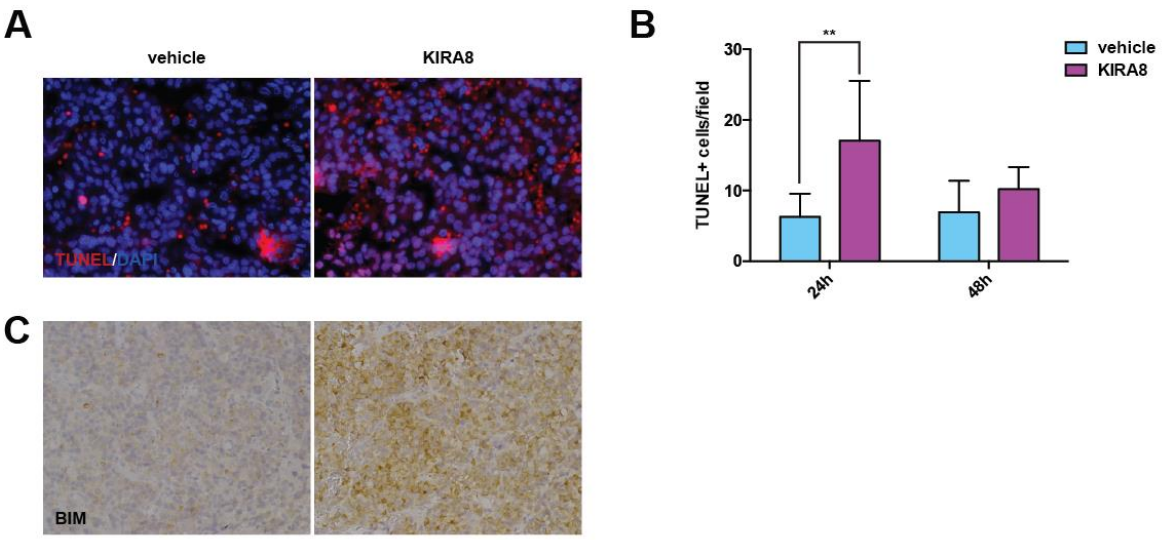

Supplemental Figure 5. KIRA8 treatment decreases tumor burden by increasing apoptosis *in vivo*.
A. Representative images of INS-1 FRT/TO xenograft tumors from animals treated with either vehicle or KIRA8 for 24h after 2 weeks of tumor growth. Tumor sections were stained for TUNEL and DAPI. Blue=DAPI. Red=TUNEL. B. Number of TUNEL-positive cells per field. 4-5 samples were stained per group, and at least 5 high-powered fields (40x magnification) were imaged per sample. p=0.0085. C. Tumor sections were stained for BIM. 40x magnification.

Publishing Agreement

It is the policy of the University to encourage the distribution of all theses, dissertations, and manuscripts. Copies of all UCSF theses, dissertations, and manuscripts will be routed to the library via the Graduate Division. The library will make all theses, dissertations, and manuscripts accessible to the public and will preserve these to the best of their abilities, in perpetuity.

I hereby grant permission to the Graduate Division of the University of California, San Francisco to release copies of my thesis, dissertation, or manuscript to the Campus Library to provide access and preservation, in whole or in part, in perpetuity.

Author Signature  Date 4/27/17